Review

Activatable fluorescent probes for atherosclerosis theranostics

Yuanyuan You,[2,4] Chengwei Tang,[1,4] Songling Lin,[2] Wenman Li,[2] Yuchao Li,[1] Dingyuan Yan,[3] Dong Wang,[3] and Xiaohui Chen[1,*]

SUMMARY

The onset of atherosclerosis (AS) is insidious, and early stage patients have atypical clinical symptoms. After being diagnosed in late stage, it is often prone to sudden and fatal cardiovascular events. Therefore, it is highly desirable to develop precise and efficient diagnosis and therapy strategies of AS. Benefiting from high signal-to-noise ratio, low detection limit, high specificity and sensitivity, a series of activatable fluorescent probes based on atherosclerotic microenvironment have emerged for identification and treatment of AS. In this review, we focus on the atherosclerotic microenvironment and briefly summarize the correlation between the structural transformation and fluorescence signal changes of mono-/double-activatable fluorescent probes upon biomarkers stimulation. Moreover, their cutting-edge progress for AS theranostics is described. Finally, the outlook for activatable theranostic probes based on atherosclerotic microenvironment is discussed to aim at promoting innovative research in imaging-guided precise AS therapy.

INTRODUCTION

Atherosclerosis (AS) is one of the most common cardiovascular diseases, and its high morbidity and mortality remain an important cause of death worldwide.[1–3] Due to no obvious symptoms in early stage, AS cannot be diagnosed promptly and accurately.[4] Plaques in arteries gradually accumulate to induce decrease in blood flow, which can lead to sudden and fatal cardiovascular events, including plaque bleeding, myocardial infarction, stroke, heart failure, and even sudden cardiac death.[5] Moreover, due to poor eating habits, AS has become younger in recent years, and many patients have experienced their first myocardial infarction at the age of 30–40.[6] In view of the increasingly severe situation, it is highly desirable to develop precise and efficient theranostic strategies.

Recently, a variety of imaging techniques in clinical practice have been used to diagnose AS include magnetic resonance imaging (MRI),[7] computed tomography (CT),[8] optical coherence tomography (OCT),[9] intravascular ultrasound (IVUS),[10] and positron emission tomography (PET).[11] While these techniques can provide an intricate evaluation of AS characteristics, they have respective and collective limitations including poor spatiotemporal resolution, low sensitivity, dangerous radiation, time-consuming, expensive, and so forth.[12–14] Fortunately, fluorescence imaging has the advantages of high spatiotemporal resolution, high sensitivity, simple operation, non-invasiveness, and *in situ* real-time monitoring, which has been widely used for AS imaging.[15–17] To date, a series of "always-on" fluorescent probes have been used for AS bioimaging, but their further applications in clinical practice are seriously limited due to nonspecific imaging of other tissues, poor signal-to-noise ratio, low specificity and sensitivity, and so forth.[18,19]

Compared with "always on" fluorescent probes, activatable fluorescent probes can transform from a weakly emissive or dark state to a bright fluorescent state upon biomarkers activation in the special microenvironment, which can significantly improve the sensitivity, detection limit, and signal-to-noise ratio of imaging in a fluorescence turn-on manner.[20–24] Moreover, activatable fluorescent probes can also achieve significant red shift or blue shift of fluorescence emission, and utilize ratiometric fluorescent imaging to improve diagnostic accuracy.[25] Furthermore, activatable fluorescent probes do not need to minimize background signals by removing nonspecific probes in normal tissues to improve signal-to-noise ratio.[26] In addition, activatable fluorescent probes are able to convert chemotherapy/phototherapy from inert to active, thereby improving the accuracy of treatment and reducing systemic toxicity.[14] Therefore, activatable fluorescent probes provide a new strategy for precise AS theranostics.

Atherosclerotic microenvironment is a highly complex physiological milieu, such as specific enzymes, high levels of reactive oxygen species (ROS) and reactive nitrogen species (RNS), weakly acidic, lipids, protein phosphorylation, which play an important role in its initiation, progression, and complications of AS (Figure 1).[12] Chronic inflammation can induce the formation of atherosclerosis. Under inflammatory microenvironment, activatable macrophages and neutrophils are able to generate a variety of enzymes into the physiological environment

[1]Institute of Laboratory Medicine, School of Medical Technology, Guangdong Medical University, Dongguan 523808, China
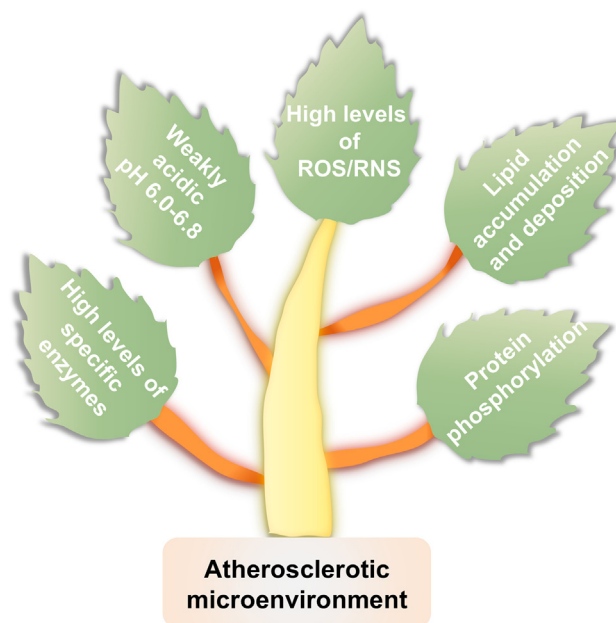[2]School of Pharmacy, Guangdong Medical University, Dongguan 523808, China
[3]Center for AIE Research, College of Materials Science and Engineering, Shenzhen University, Shenzhen 518060, China
[4]These authors contributed equally
*Correspondence: xhchen@gdmu.edu.cn
https://doi.org/10.1016/j.isci.2024.111009

Figure 1. Schematic diagram of atherosclerotic microenvironment

of plaques, such as cysteine proteases and β-galactosidase, leading to the increased level of specific enzymes.[17] Moreover, activatable macrophages can also induce the overgeneration of ROS and RNS, such as H_2O_2, $\cdot O_2^-$, HClO, HBrO, $ONOO^-$, NO, and so forth, which involve several redox systems and exacerbate plaque progression.[27,28] In addition, the weakly acidic nature of the atherosclerotic microenvironment is primarily attributed to several factors, including hypoxic condition, increased lactate production, oxidative stress and abundant activatable macrophages and neutrophils.[13] The accumulation of lipids in the atherosclerotic microenvironment is caused by the interaction of a series of factors such as endothelial dysfunction, lipid retention and oxidation, immune cell activation, and foam cell formation, *etc*.[29] Protein phosphorylation plays an important role in regulating and controlling protein activity and function. Inflammation tissues of AS is often accompanied by abnormal phosphorylation levels.[30] Understanding formation mechanisms of atherosclerotic microenvironment is crucial for developing theranostic strategies to identify and treat AS.

In recently years, a series of activatable fluorescent probes based on atherosclerotic microenvironment have emerged for identification and treatment of AS. In this review, we mainly summarize the transformation mechanisms of chemical structures and corresponding fluorescence signal changes of activatable fluorescent probes based on atherosclerotic microenvironment in AS theranostics. Its main features include: (1) the impact of the structural transformation of mono-activatable fluorescent probes based on single microenvironmental biomarker on fluorescence signal changes; (2) structural transformation mechanisms, fluorescence signal transformation of dual-activatable fluorescent probes based on two microenvironmental biomarkers are described; and (3) the activatable fluorescent probes for effective AS therapy is also described. (4) The challenges and prospects of activatable theranostic probe for imaging-guided precise AS therapy are discussed.

MONO-ACTIVATABLE FLUORESCENT PROBES FOR IMAGING OF AS
Enzyme-activatable fluorescent probes

Monocytes, macrophages and neutrophils in atherosclerotic microenvironment can abnormally secrete specific enzymes, including cathepsins, β-galactosidase, γ-glutamyl transpeptidase (GGT), and so forth.[31] Therefore, enzyme-activatable probes enable specific imaging of AS lesions.[17]

Atherosclerotic microenvironment exhibits an upregulation of cathepsins, particularly cathepsin K (CTK) and cathepsin B (CTB), which can mediate the erosion and rupture of vulnerable plaques.[32] Cathepsins-activatable fluorescent probes can achieve the transition from an initial dark state to a highly bright state showing excellent signal-to-noise ratio, which are particularly suitable for turn-on fluorescence imaging of AS. Jaffer et al. developed a CTK-activatable NIRF probe showing non-emission in absence of CTK, which can present bright red fluorescence after treatment with CTK (Figure 2A).[33] Moreover, NIRF probe could effectively light up the carotid specimen in human carotid atherosclerotic lesions, showing *in situ* monitor of CTK activity in AS lesions (Figure 2B). Moreover, Narita et al. designed and synthesized a macrophage-targeted and CTB-activatable fluorescent nanoprobe P-ICG2-PS-Lip to achieve light-up imaging of atherosclerotic plaques (Figures 2C–2E).[34] The P-ICG2-PS-Lip can specifically target macrophages by utilizing the interaction between ligands and receptors, and subsequently turn on fluorescence signal under the action of lysosomal CTB. In animal experimental model (ApoE-knockout atherosclerotic model mice),
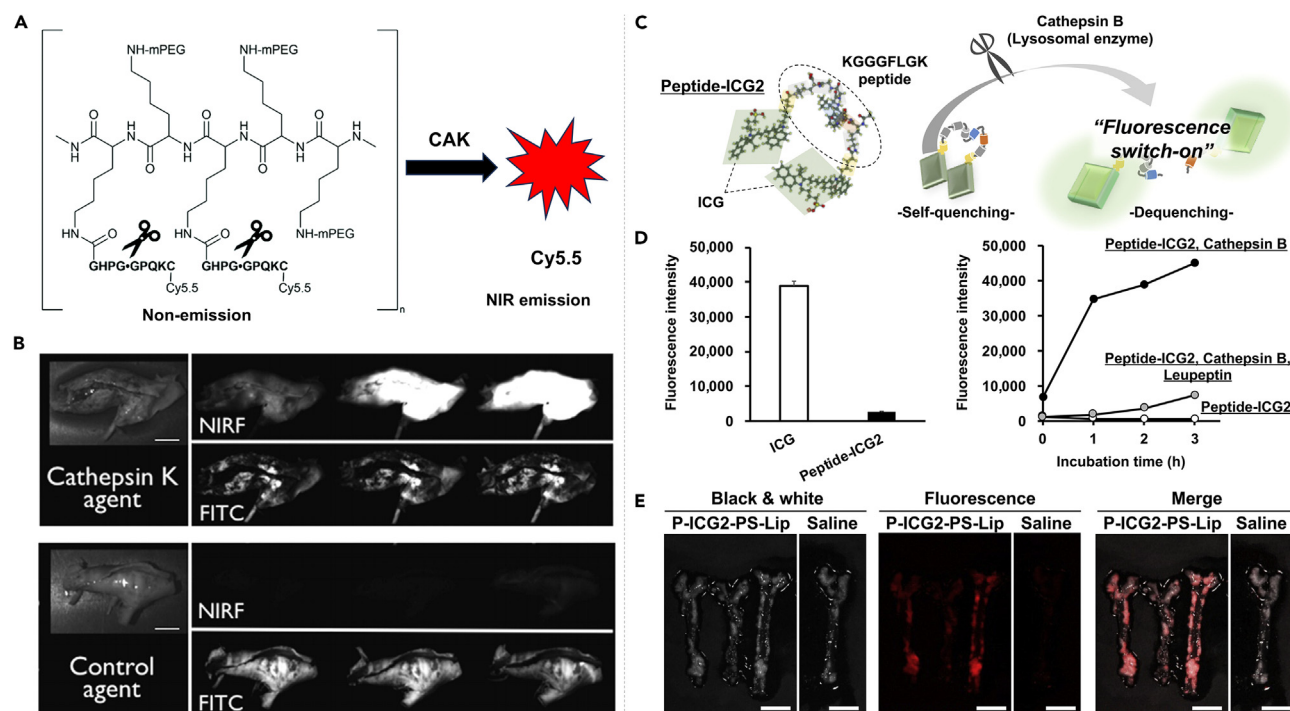
Figure 2. Cathepsins-activatable fluorescent probes for imaging of AS

(A) The Chemical structures of CTK-activatable NIRF probe.

(B) Optical imaging of a carotid specimen in human carotid atherosclerotic lesions; Reproduced with permission, from Jaffer et al.[33] Copyright 2007, American Heart Association.

(C) Schematic illustration of fluorescence-switch of CTB activatable probe.

(D and E) Fluorescence intensity of Peptide-ICG2 in presence of CTB; Reproduced with permission, from Narita et al.[34] Copyright 2019, Elsevier.

the P-ICG2-PS-Lip can also light up the aortae, showing NIR fluorescence signal and a high signal-to-noise ratio. The nanoprobe is highly promising for diagnosis of atherosclerotic plaque.

Cell senescence is closely related to the occurrence and development of atherosclerosis.[35] Studies have revealed an overexpression of senescence-associated β-galactosidase (β-Gal) in senescent cells, which plays an important role in the early diagnosis of AS.[36] Chen et al. developed a β-Gal-activatable nanoprobe BOD-L-βGal-NPs composed of NIR ratiometric probe and amphiphilic polymers PLGA, which can effectively real-time monitor the β-Gal activity in AS model mice (Figure 3A).[37] In presence of β-Gal, a decreased absorption intensity was exhibited at 500 nm (a special absorption peak of BOD-L-βGal), while a gradually increased absorption intensity was observed at 650 nm (a special absorption peak of BOD-L-SH), which can be caused by the effective activation of BOD-L-βGal (Figure 3B). Moreover, the maximum fluorescence emission peak of BOD-L-βGal showed significant red-shift from 500 nm to 730 nm (Figures 3C and 3D), which is especially suitable for *in vivo* tissue imaging due to deep tissue penetration ability. The BOD-L-βGal-NPs can be taken up by aging VSMC induced by Ang II (β-Gal inducer) showing strong red fluorescence signal, while a weak fluorescence intensity was observed for normal VSMC (Figure 3E). Compared with normal mice, the AS model mice showed a strong NIR fluorescence signal with excellent signal-to-noise ratio after treatment with BOD-L-βGal-NPs (Figure 3F). To further investigate the diagnosibility of BOD-L-βGal-NPs for aging atherosclerotic vessels, the aortas of normal and AS mice were extracted for fluorescence imaging. As shown in Figure 3G, AS model mice had obvious fluorescence signal in aortas, while the normal mice showed non-fluorescence signal. Therefore, the β-Gal-activatable nanoprobe is highly potential for the early diagnosis and therapy of AS.

ROS-activatable fluorescent probes

ROS refers to the highly reactive free radicals formed on the unpaired electrons of oxygen, such as hydroxyl radical ($\cdot$OH), superoxide anion ($\cdot O_2^-$), singlet oxygen ($^1O_2$).[38–40] Macrophages in atherosclerotic microenvironment can produce a large amount of ROS.[41–44] Therefore, ROS-activatable probes are very promising for targeted imaging of AS.

H₂O₂-activatable fluorescent probes

Inflamed areas of AS can generate rich H_2O_2 as a biomarker.[45] H_2O_2-activatable photoacoustic probes have been used for bioimaging of AS,[41] while they exhibit the drawback of being time-consuming to collect signals. H_2O_2-activatable fluorescent probes have been developed
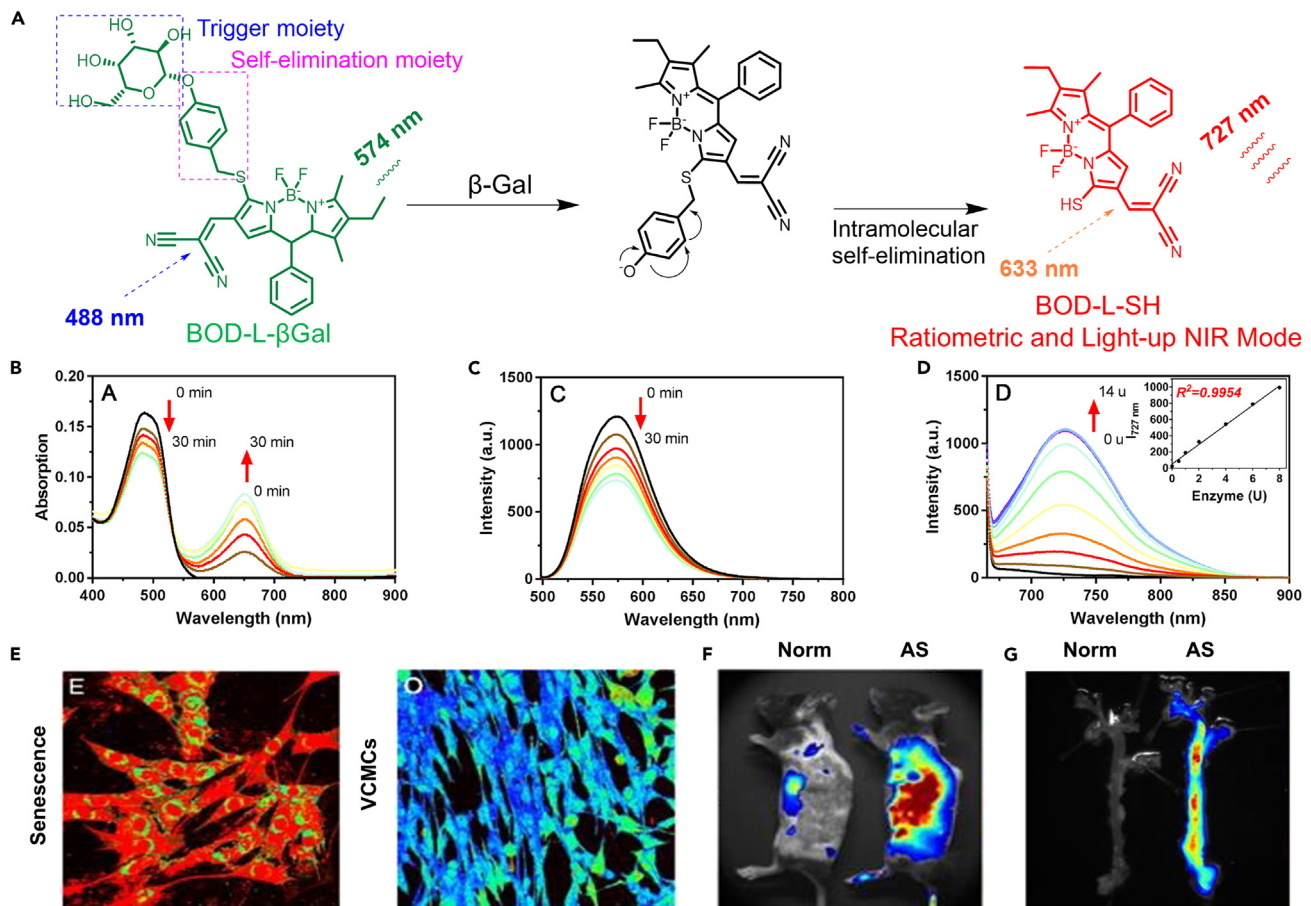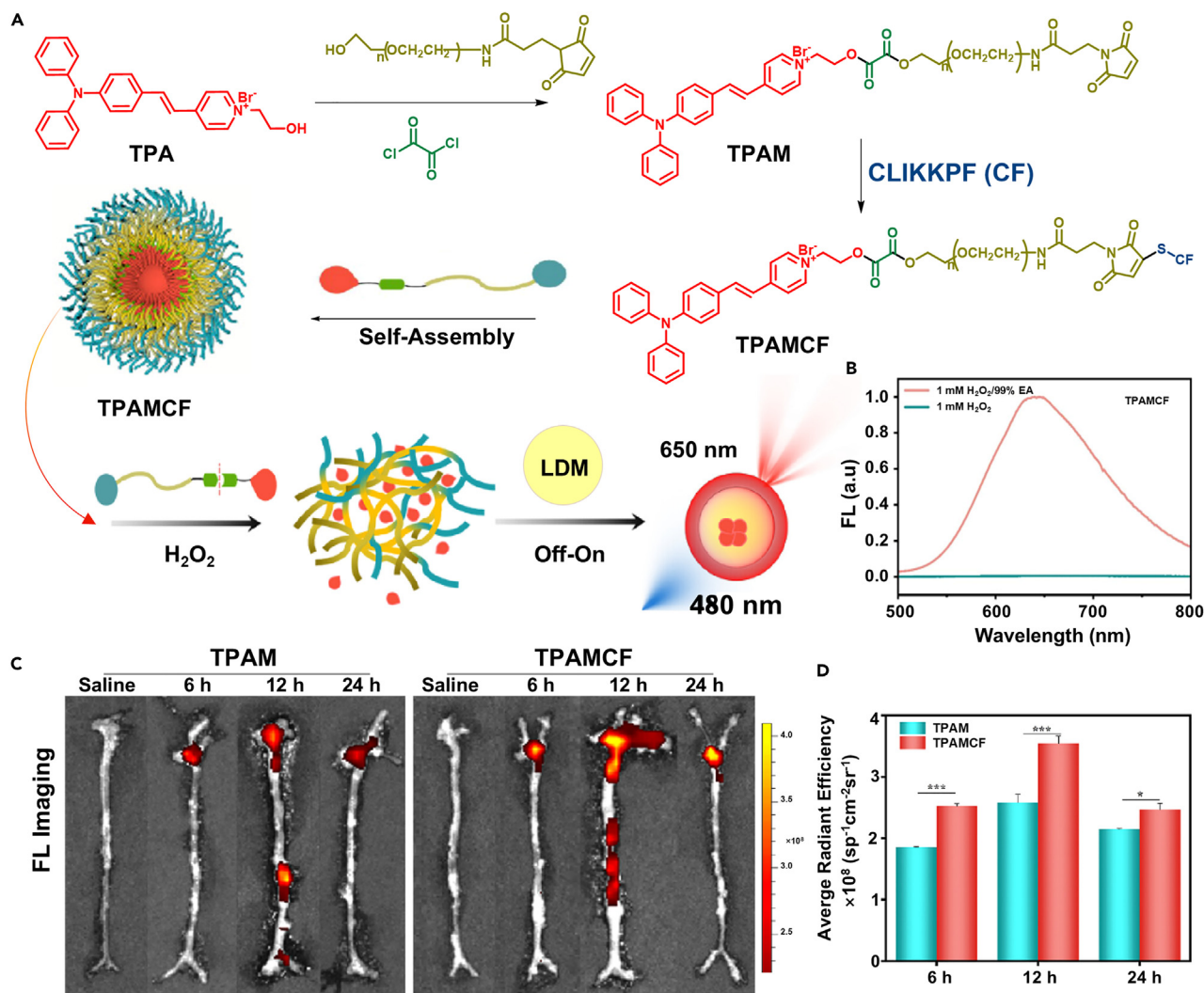
Figure 3. β-Gal-activatable fluorescent probe for imaging of AS

(A) Chemical structures of BOD-L-βGal before and after β-Gal activation; Time dependence of (B) absorption and (C–D) PL spectra of BOD-L-βGal in presence of β-gal; (E) Ratiometric images of Ang II-treated VSMCs and primary VSMCs; Fluorescence images of (F) normal and AS mice and (G) aortic arch of the normal and Ange II-treated mouse after the injection of BOD-L-βGal-NPs; Reproduced with permission, from Chen et al.[37] Copyright 2020, American Chemical Society.

for diagnosis of AS. Liu et al. devised the H_2O_2-activatable fluorescent probe TPAMCF composed with TPA with aggregation-induced emission properties, H_2O_2-responsive maleimide (polyethylene glycol) hydroxyl, and CLIKKPF peptide for targeting foam cell phosphatidylserine, which can be used for diagnosis of atherosclerotic plaques (Figure 4A).[46] After being self-assembled into nanoparticles in aqueous solution, TPAMCF in co-solvent of H_2O_2/EA (f_{EA} = 99%) showed a significantly increased fluorescence signal upon activation by H_2O_2 due to the formation of aggregates of TPA in low-polarity microenvironment (Figure 4B), indicating that TPAMCF is particularly suitable for bioimaging of atherosclerotic plaques. Utilizing a ligand-receptor interaction strategy, the nanoprobe TPAMCF could effectively accumulate in the atherosclerotic plaque lesions. Subsequently, the nanoprobe TPAMCF disassembled upon activation by H_2O_2 in the lesion microenvironment, and then TPA can be released to effectively target lipid droplets (LDs) and light up the foam cells in atherosclerotic plaques. As showed in Figures 4C and 4D, ApoE$^{-/-}$ mice were fed with high-fat diet for 8 mouths to induce atherosclerosis as *in vivo* AS model. The aortas of mice injected with drugs at different time points were excised and a significantly stronger fluorescence signal was observed for TPAMCF NPs group compared with that of TPAM NPs. Therefore, TPAMCF as a precise and noninvasive imaging modality is highly promising for assessing the progression and prognosis of AS. To effectively improve accumulation at atherosclerotic plaque sites, Kong et al. synthesized H_2O_2-activatable nanoprobe R-Lipo@HDB/CH1055 containing two organic small molecule probes (HDB and CH1055).[47] The fluorescence intensity ratio of HDB to CH1055 (F_{710}/F_{940}) was linearly related to the H_2O_2 levels (10–100 μM), which can more accurately identify the location of atherosclerotic plaques and effectively avoid the related interference caused by probes accumulation or metabolism.

HClO-activatable fluorescent probes

Upregulation of HClO levels for foam cells in atherosclerotic microenvironment is considered as an important causative factor in the development of AS, which can effectively destroy endothelial function, oxidative lipoprotein, and enhance the plaque instability.[48] Therefore, the development of highly sensitive HClO-activatable fluorescent probes is of great significance for precise imaging and auxiliary diagnosis. Ye

Figure 4. H$_2$O$_2$-activatable fluorescent probe for imaging of AS
(A) Chemical structures of TPAMCF and H$_2$O$_2$-activatable AIE imaging.
(B) PL spectra of TPAMCF treated with H$_2$O$_2$ in presence of EA.
(C) Fluorescence images of the same whole aorta isolated from ApoE$^{-/-}$ mice model of AS *in vivo*, sacrificed at 6, 12, or 24 h post intravenous injection of saline, TPAM NPs, or TPAMCF NPs.
(D) The corresponding average FL intensity; Reproduced with permission, from Liu et al.[46] Copyright 2023, American Chemical Society.

et al. synthesized a HClO-activatable single-molecule fluorescent probe MTB-B-CF3 based on the HClO-responsive *p*-methylthio-phenylene moiety and BODIPY framework, which can be used to effectively detect and identify atherosclerotic plaques (Figure 5A).[49] With the increase of HClO concentration, the fluorescence intensity at 600 nm of MTB-B-CF3 gradually increased, while a decreased fluorescence intensity at 670 nm was observed, which can be attributed to the effective transformation from thioether into sulfoxide on MTB-B-CF3 upon HClO activation (Figure 5B). To study the bioimaging and recognition ability of MTB-B-CF3 on atherosclerosis *in vivo*, the AS model was constructed using ApoE$^{-/-}$ mice fed high-fat diet for 12 weeks, and healthy C57BL/6J mice served as control group. MTB-B-CF3 and Ac-LDL formed nanoprobes through self-assembly, which can target macrophages and improve blood circulation *in vivo*. Furthermore, the nanoprobe can effectively accumulate in atherosclerotic plaques, where Ac-LDL was metabolized by foam cells and subsequently transferred into LDs, while the released MTB-B-CF3 achieved light-up imaging of lipid droplets. The yellow and red fluorescence signal in the superficial carotid plaque region could be observed in the mice model of AS *in vivo*, while a weak fluorescence signals was exhibited in the control C57BL/6J mice (Figures 5C and 5D).

In order to real-time monitor the development of AS, Ji et al. further synthesized a HClO-activatable and foam cells-targeted amphiphilic fluorescent probe BI-PEG-PSBP, which can self-assembly into BI-PEG-PSBP nanoparticles (NPs) with an average size of 250 nm (Figure 5E).[50] Moreover, BI-PEG-PSBP NPs could be hydrolyzed and transformed into B-CF3 with green fluorescent emitting under the action of HClO,
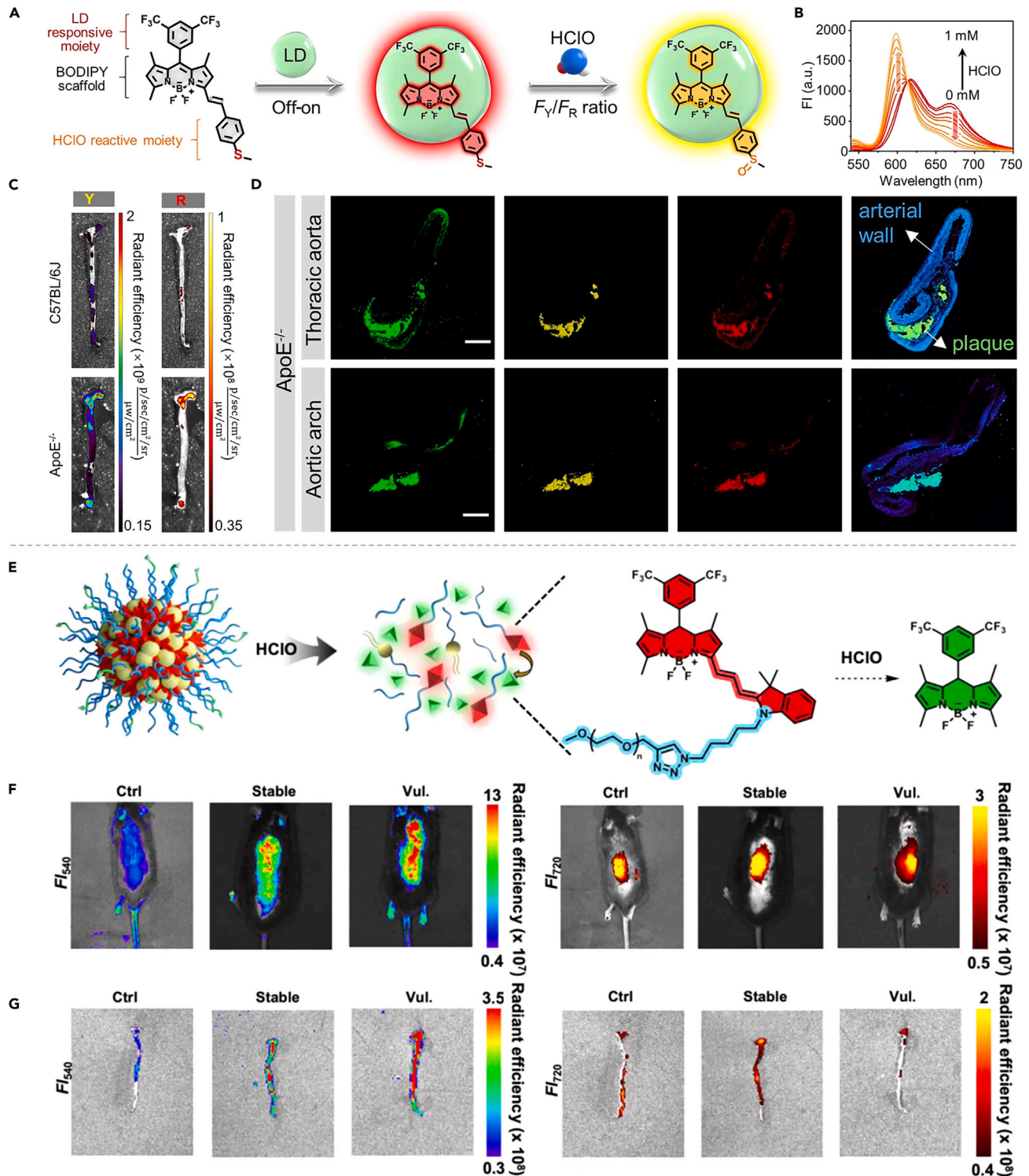
Figure 5. HClO-activatable fluorescent probes for imaging of AS

(A) Chemical structures of MTB-B-CF$_3$ before and after HClO activation.

(B) PL spectra of MTB-B-CF$_3$ treated with different concentration of HClO.

(C) *Ex vivo* fluorescence images of aortas and main organs in C57BL/6J (control) and ApoE$^{-/-}$ mice after intravenous injection of nanoprobe for 24 h; Reproduced with permission, from Ye et al.[49] Copyright 2022, Wiley.

Figure 5. Continued
(D) The fluorescence imaging sections.
(E) Schematic illustration of HClO-activatable BI–PEG-PSBP NPs dissociation.
(F and G) Fluorescence imaging of (F) the model mice at the carotid regions and (G) the corresponding aortas; Reproduced with permission, from Ji et al.[50]
Copyright 2024, American Chemical Society.

which can specifically target LDs and light up foam cells. After intravenous injection of BI–PEG-PSBP NPs for 12 h, the fluorescence intensity at 540 nm increased with the progression of atherosclerotic plaques, indicating that BI-PEG-PSBP NPs could be effectively transformed into B-CF3 showing green fluorescence emission under the activation of HClO (Figures 5F and 5G). Moreover, the circulating EVs stained by B-CF3 can be monitored through fluorescence spectrometer or microplate reader in the laboratory, which is particularly suitable for the early diagnosis and real-time monitoring of the development of AS.

ONOO⁻-activatable fluorescent probes

Foam cells in atherosclerotic microenvironment are one of biomarkers in advanced AS, and ONOO⁻ is mainly formed in the lipid droplets (LDs) of foam cells.[51–53] Therefore, the ONOO⁻-activatable fluorescent probes are suitable for the diagnosis of AS at the early stage. Zhang et al. designed and synthesized a new kind of rhodamine derivative (ON-RB) based on the dibenzo[1,4]oxazepine core, which can effectively transform into oxazine 1 via reconstruction of the π-conjugation (Figure 6A).[54] As shown in Figures 6B and 6C red-shifted absorption and strong fluorescence intensity at 672 nm for ON-RB was observed in presence of ONOO⁻, which was caused by the generation of oxazine
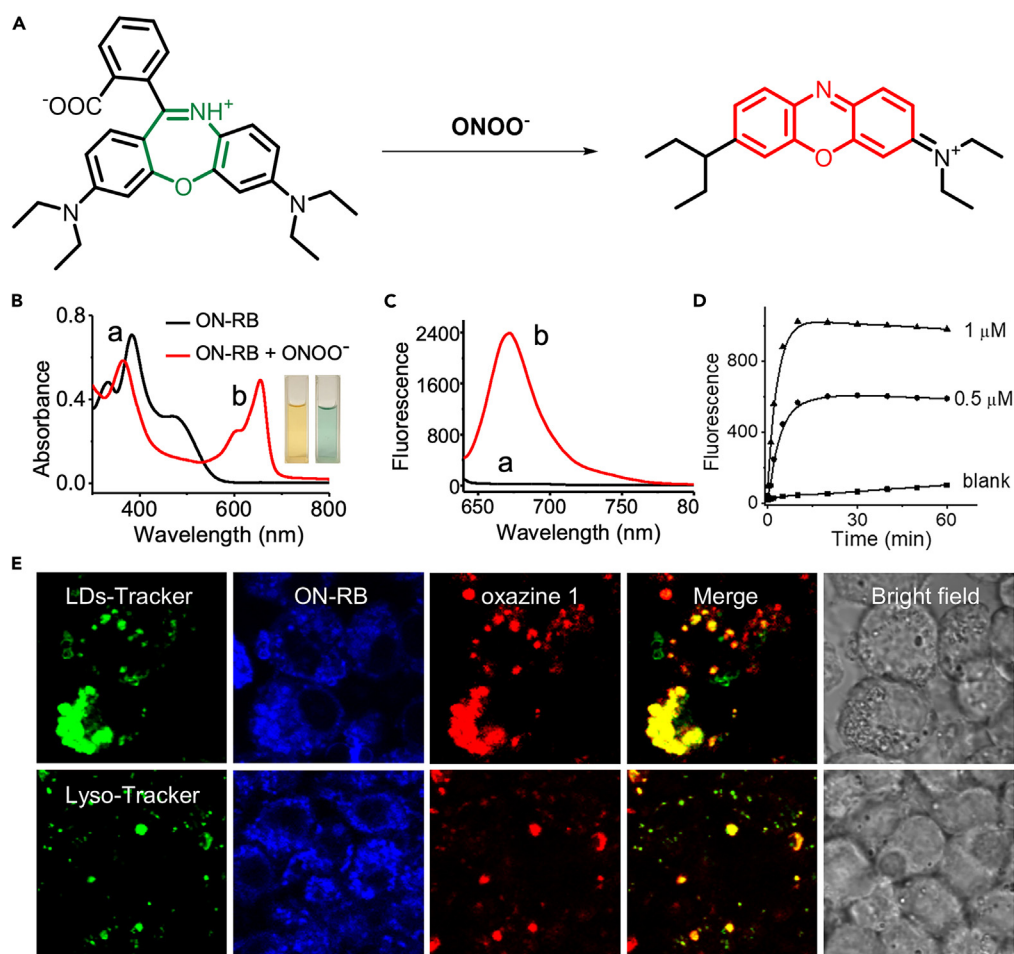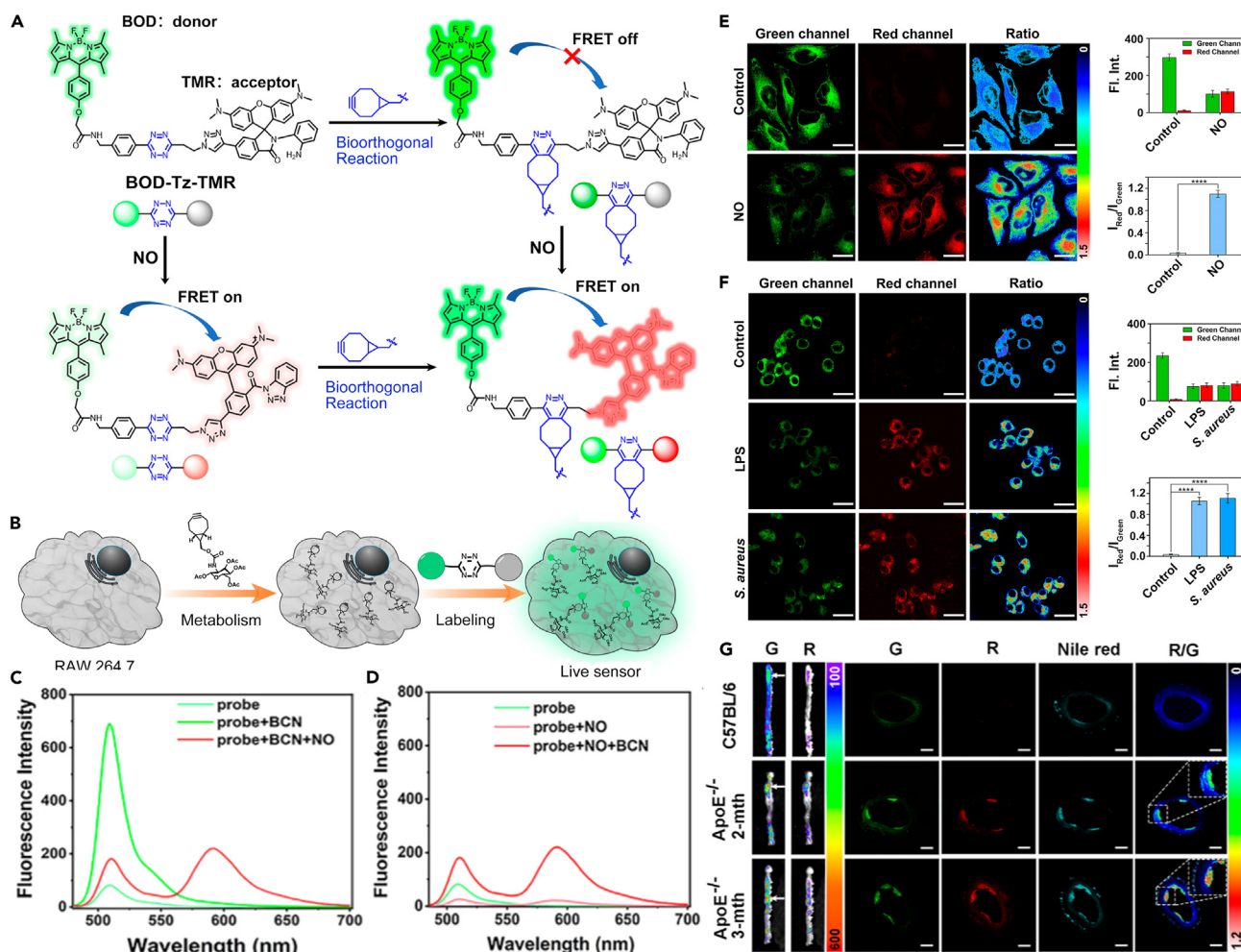

Figure 6. ONOO⁻-activatable fluorescent probe for imaging of AS
(A) Chemical structures of ON-RB before and after ONOO⁻ activation.
(B) The UV–vis absorption and (C) PL spectra of ON-RB treated with/without ONOO⁻.
(D) Time dependence of PL intensity of ON-RB treated with different concentration of ONOO⁻.
(E) CLSM images of foam cells co-stained by ON-RB and LDs-Tracker/Lyso-Tracker. Reproduced with permission, from Zhang et al.[54] Copyright 2022, Elsevier.

Figure 7. NO-activatable fluorescent probe for imaging of AS

(A) Chemical structures of BOD-Tz-TMR before and after NO activation.

(B) Mechanism of macrophages labeled with "live probe" through bio-orthogonal reaction.

(C and D) PL spectra of ON-RB in presence of BCN and/or NO.

(E and F) CLSM images of (E) HeLa treated with exogenous NO and (F) RAW 264.7 treated with endogenous NO.
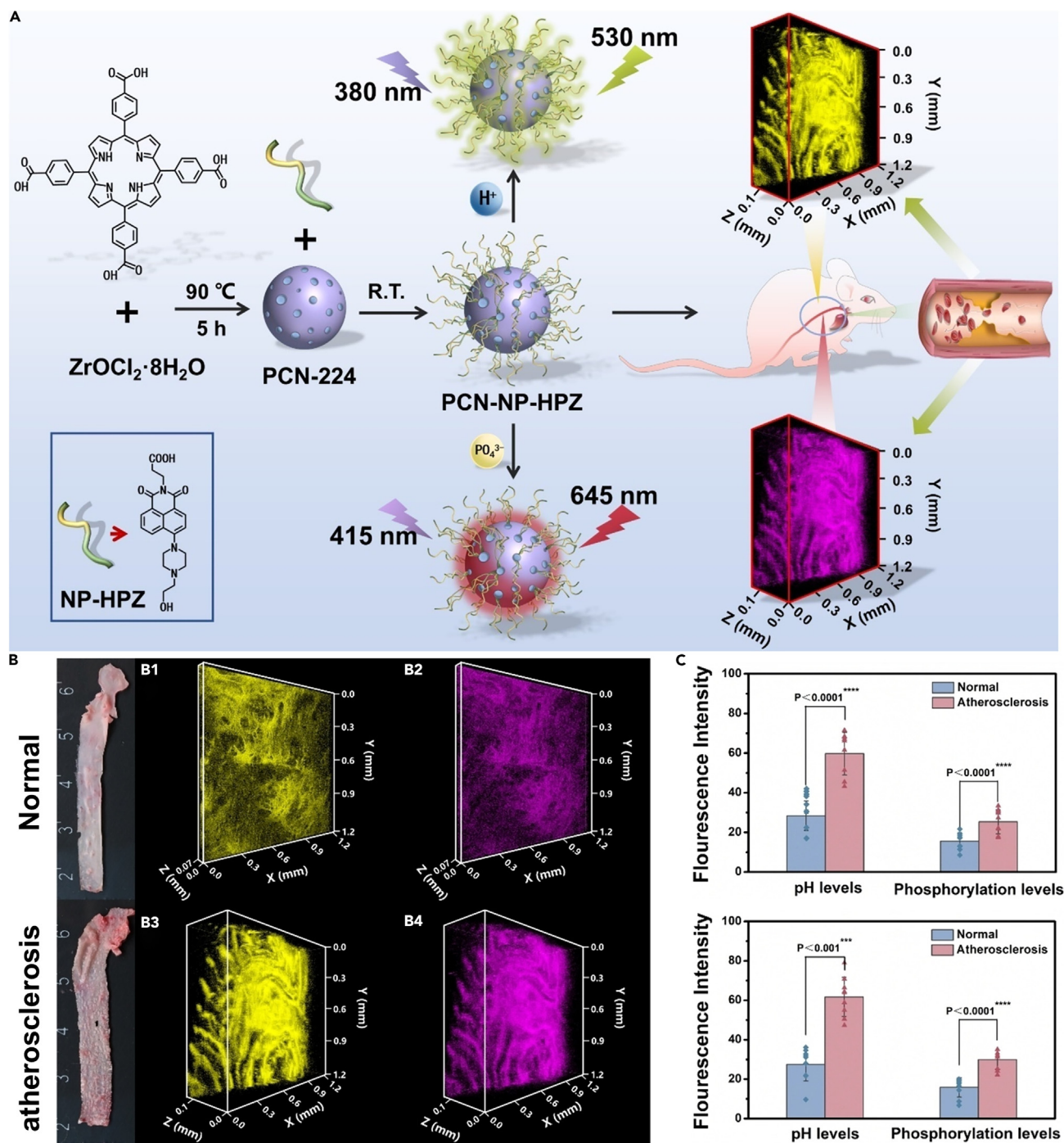
(G) *Ex vivo* fluorescence images of atherosclerotic plaque and sections of the thoracic aorta in C57BL/6J and ApoE$^{-/-}$ mice; Reproduced with permission, from Zhou et al.[55] Copyright 2023, American Chemical Society.

1 with an increased π-conjugation system. Moreover, ON-RB can detect ONOO$^-$ with high selectivity and sensitivity in physiological environments (Figure 6D). Furthermore, a high overlap (0.72) was observed between red fluorescent signal of ON-RB and green fluorescent signal of LDs-Tracker inside foam cells, indicating that ONOO$^-$ is mainly exhibited in the LDs of foam cells (Figure 6E). Therefore, the development of ONOO$^-$-activatable and LDs-responsive probes is more suitable for AS theranostics.

NO-activatable fluorescent probes

NO is a specific marker in the formation of AS plaques, which can be used to characterize the location of AS plaques. Recently, a series of activatable fluorescent probes were developed for *in vitro* detection of NO. However, lack targeting ability for *in vivo* mice model limits widespread clinical translation. To tackle these challenges, Zhou et al. designed and developed a "live sensor" composed of macrophages and NO-activatable FRET probe BOD-Tz-TMR, which can specifically target the AS plaques and effectively monitor endogenous NO level in the AS model (Figures 7A and 7B).[55] The probe BOD-TZ-TMR can react with BCN and NO for macrophages labeling by biorthogonal reaction and NO detection, respectively (Figures 7C and 7D). *In vitro* cell experiments confirmed that BOD-TZ-TMR can effectively label HeLa cells and macrophages RAW 264.7, which could be used to study the activation properties of the probe by exogenous and endogenous NO, respectively. As shown in Figures 7E and 7F, the two live sensors with high the stability and sensitivity can effectively detect NO level at the *in vitro* model. To investigate diagnostic ability of "live sensor" for NO during the formation of atherosclerotic plaques in mice models,

Figure 8. The pH- and phosphorylation-activatable fluorescent probe for imaging of AS

(A) Schematic illustration of PCN-NP-HPZ for fluorescence imaging of the Atherosclerotic mice.

(B) Two-photon fluorescence imaging of vascular inner wall of normal mice and early atherosclerotic mice.

(C) The changes of fluorescence intensity of PCN-NP-HPZ on pH level and phosphorylation level in the thoracic and abdominal aorta; Reproduced with permission, from Li et al.[56] Copyright 2023, Wiley.

Apolipoprotein E-deficient (ApoE$^{-/-}$) mice by high-fat feeding were used for developing *in vivo* AS model. The *ex vivo* imaging was performed 36 h after tail vein injection of RAW 264.7 cells labeled with BOD-TZ-TMR (Figure 7G). The results confirmed that BOD-TZ-TMR can discover plaques and identify the stages of AS plaques by quantitatively detecting endogenous NO. This study innovatively utilized
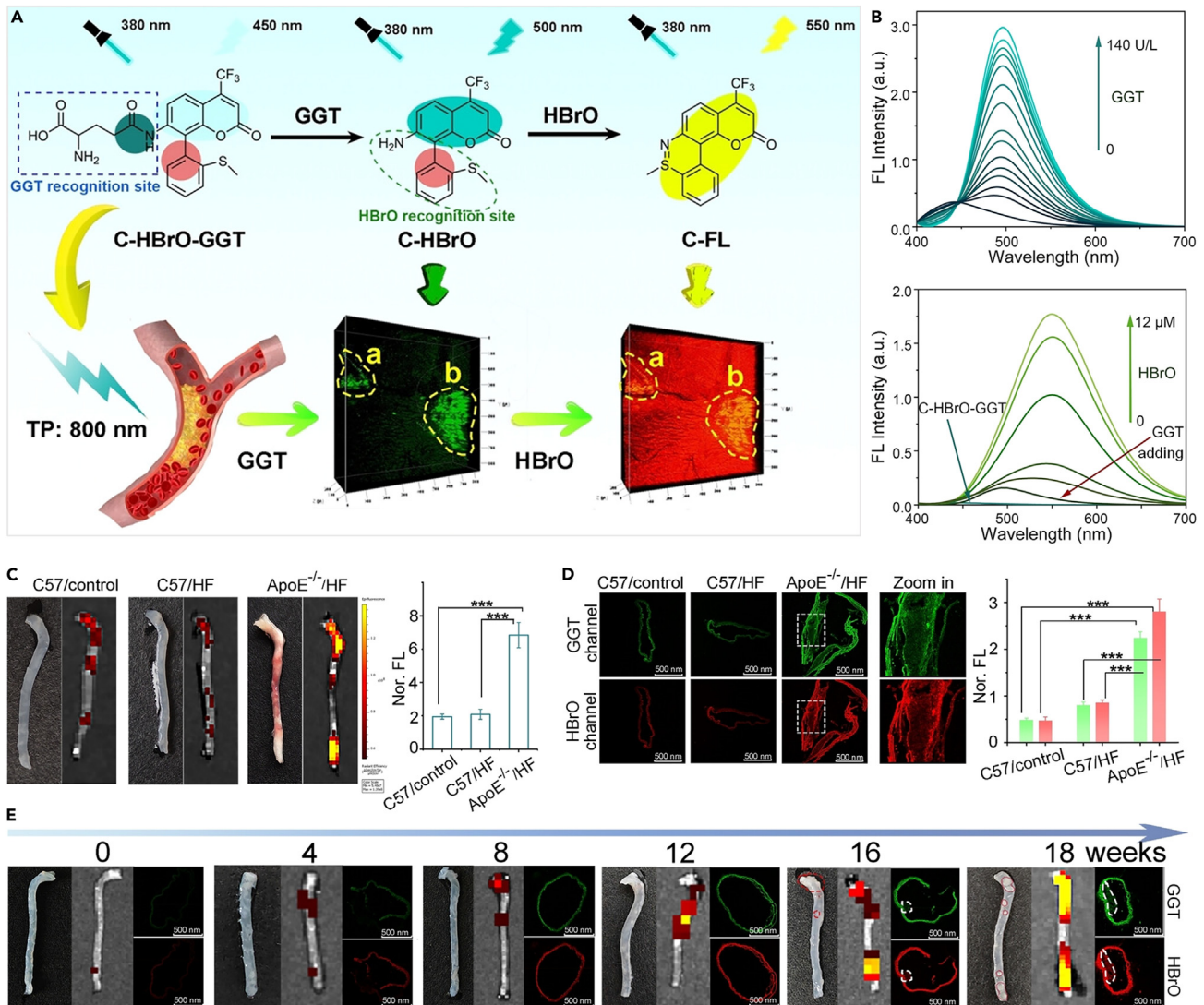
Figure 9. GGT- and HBrO-activatable fluorescent probe for imaging of AS

(A) Schematic illustration of GGT- and HBrO-activatable probe C-HBrO-GGT for fluorescence imaging of AS.

(B) PL spectra of C-HBrO-GGT treated with different concentration of GGT or HBrO.

(C) *Ex vivo* fluorescence imaging of Sequence-activatable probe C−HBrO-GGT in aortas.

(D) CLSM images of frozen sections from aorta treated with C−HBrO-GGT.

(E) *In vivo* fluorescence and CLSM images of C−HBrO-GGT in aortas; Reproduced with permission, from Wang et al.[60] Copyright 2024, Wiley.

macrophages as carriers to directly detect endogenous NO generation during the formation of AS, which has great potential and advantages for diagnosis and treatment of AS in the future.

DUAL-ACTIVATABLE FLUORESCENT PROBE FOR IMAGING OF AS

Compared with mono-activatable fluorescent probes, dual-/multi-activatable fluorescent probes can cascade activate fluorescence signal or induce a red-shift or blue-shift of fluorescence emission under the action of two biomarkers in the atherosclerotic microenvironment, which can be more effectively improve accuracy and precision of AS identification.

pH- and phosphorylation-activatable fluorescent probe

The pH changes and protein phosphorylation levels are closely related to the initiation and progression of AS. Li et al. developed a pH- and phosphorylation-activatable fluorescence probe PCN-NP-HPZ based on NP-HPZ with piperazine group and MOFs with Zr^{IV} metal node, which can be used for monitoring the pH and phosphorylation level of atherosclerosis in different stages (Figure 8).[56] The early stage of
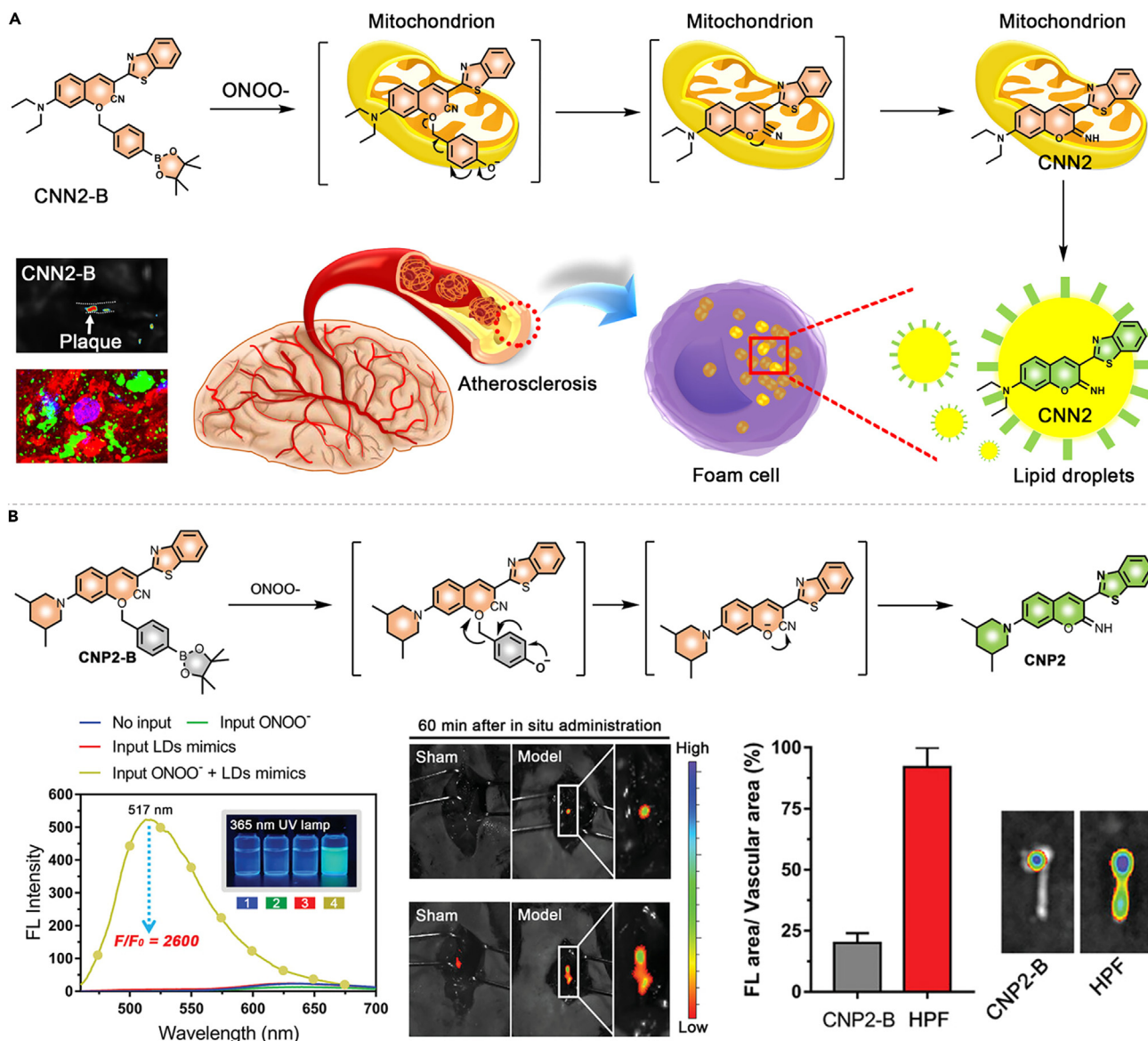
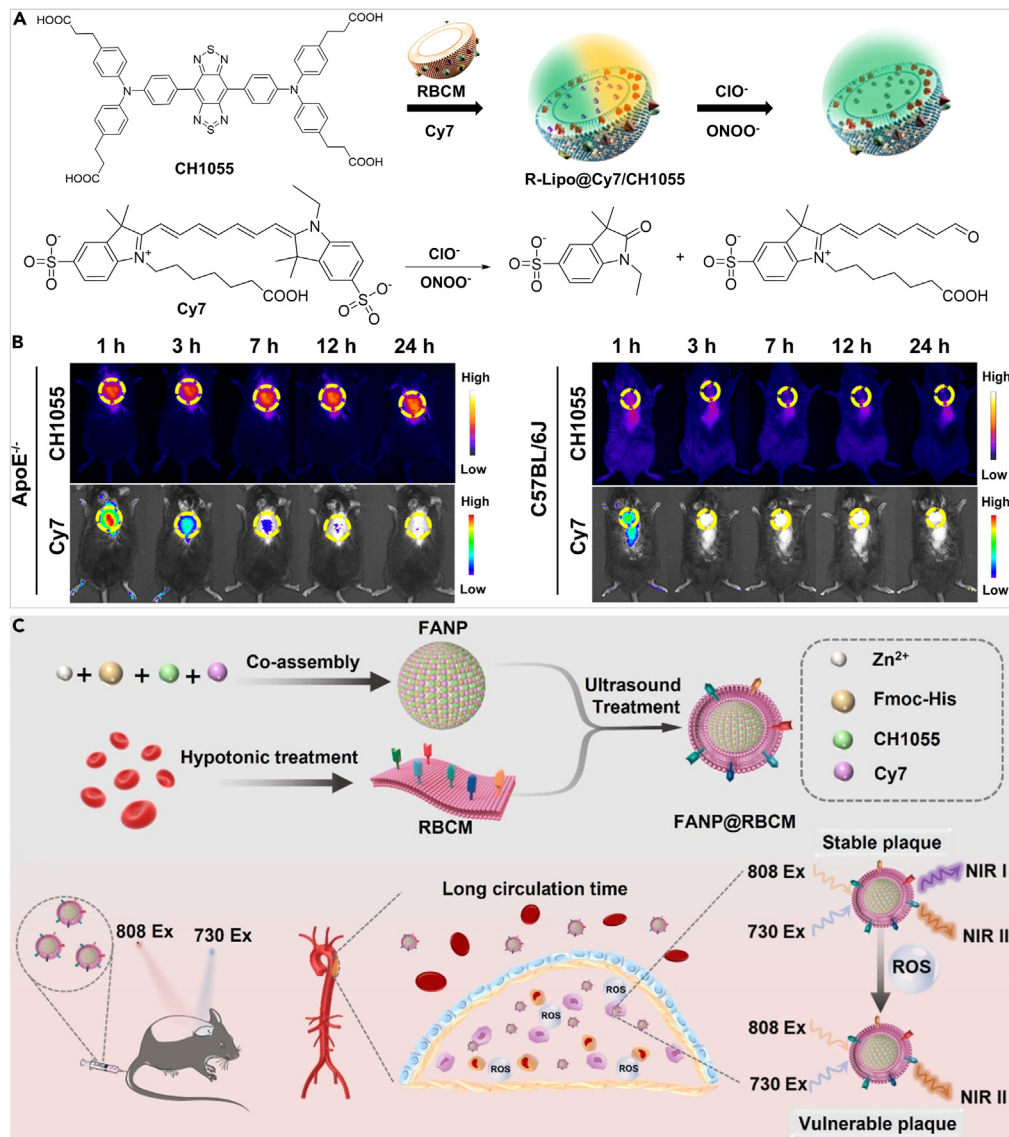**Figure 10. ONOO⁻and LDs-activatable probe for imaging of AS**

(A) Schematic illustration of ONOO⁻and LDs-activatable probe CNN2-B for fluorescence imaging of AS; Reproduced with permission, from Sang et al.[64] Copyright 2023, American Chemical Society.

(B) Schematic illustration of ONOO⁻and LDs-activatable probe CNP2-B for fluorescence imaging of AS; Reproduced with permission, from Sang et al.[65] Copyright 2023, Wiley.

AS model was established by intraperitoneal injection of VD3 and high-fat feeding. Then, the diagnostic potential of the PCN-NP-HPZ is systematically investigated via detecting the pH and phosphorylation level of blood and tissue. Compared with normal mice, the pH level of mice in the early stage of AS was lower, and phosphate level is higher. The study provides a new dual-activatable nanoprobe tool for monitoring the AS progression and studying the mechanism of action.

GGT- and HBrO-Activatable fluorescent probe

The GSH-hydrolyzed protein γ-glutamyl transpeptidase (GGT) and hypobromous acid (HBrO) are two potential biomarkers in atherosclerotic microenvironment.[57–59] In order to avoid false positive results produced by a single biomarker, Tang et al. designed and developed a GGT- and HBrO-sequentially activatable fluorescent probe C-HBrO-GGT, which can *in situ* monitor GGT activity and HBrO level in atherosclerotic sites (Figure 9A).[60] As the GGT concentration increased, the emission peak at 450 nm gradually decreased, while the emission peak at 500 nm gradually increased. Moreover, the fluorescence intensity at 550 nm of GGT-activatable C-HBrO-GGT increased with a

Figure 11. HClO- and ONOO⁻-activatable probe for imaging of AS

(A) Schematic illustration of the synthesis of HClO- and ONOO⁻-activatable probe R-Lipo@Cy7/CH1055 and chemical structures of Cy7 before and after activation.

(B) Cy7 and CH1055 fluorescence images of ApoE$^{-/-}$ and C57BL/6J mice treated with R-Lipo@Cy7/CH1055, respectively. Reproduced with permission, from Kong et al.[47] Copyright 2024, Elsevier.

(C) Schematic illustration of the synthesis of HClO- and ONOO⁻-activatable nanoprobes FANP@RBCM for identification and vulnerability risk assessment of AS. Reproduced with permission, from Kong et al.[69] Copyright 2024, American Chemical Society.

29.78-fold when the concentration of HBrO increased to 12 μM (Figure 9B). To further investigate the diagnostic ability of the dual-activatable probe for AS, the apolipoprotein E-deficient (ApoE$^{-/-}$/HF) mice by high-fat feeding were used for establishing AS model *in vivo*. C-HBrO-GGT can *in situ* real-time monitor GGT activity and HBrO levels in the blood vessels of ApoE$^{-/-}$/HF mice (Figures 9C–9E), which can effectively predict the formation of atherosclerotic plaques. This research has a highly potential to achieve imaging-guided precise AS therapy.

ONOO⁻- and LDs-Activatable fluorescent probes

ONOO⁻ and LDs are two hallmarks in atherosclerotic microenvironment.[61–63] To precisely light up atherosclerotic plaques *in vivo*, Sang et al. developed a ONOO⁻ and LDs sequentially activatable fluorescence probe CNN2-B showing intraoperative imaging of atherosclerotic plaques with a high F/F_0 ratio (Figure 10A).[64] Moreover, Sang et al. further designed and synthesized an "AND" molecular logic gate to improve
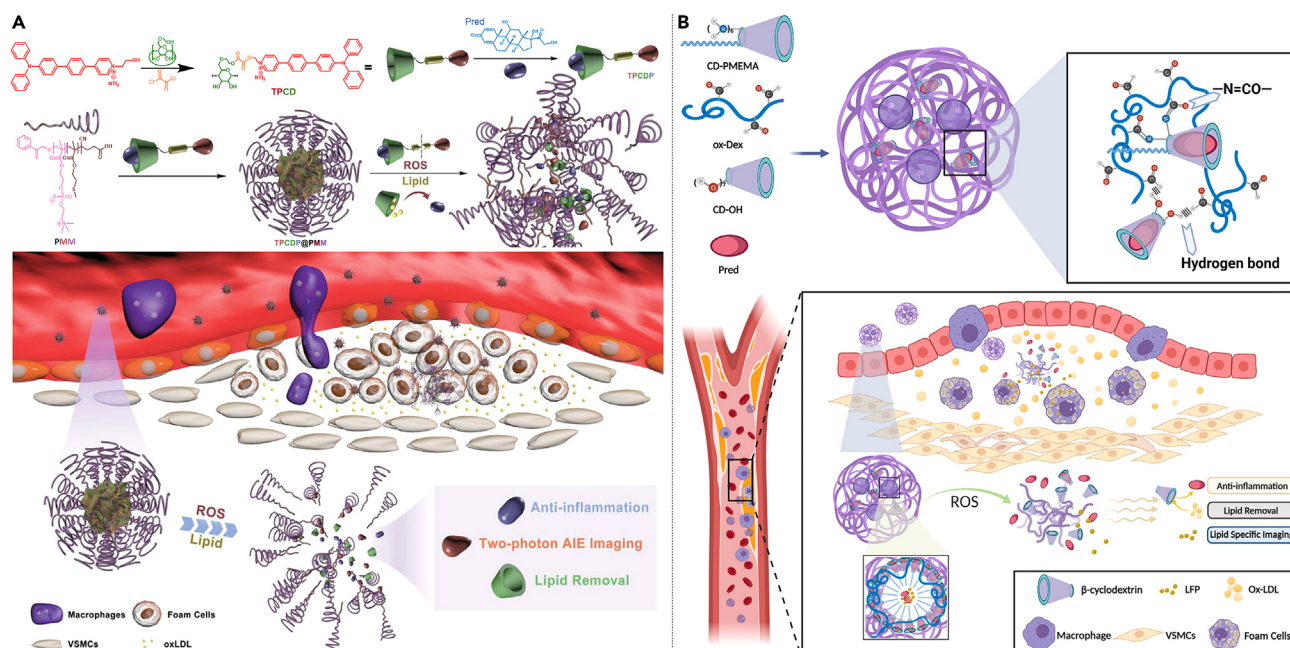
Figure 12. Lipid- and ROS-activatable probes for AS theranostics

(A) Schematic illustration of ROS responsive nanoplatform TPCDP@PMM for AS theranostics. Reproduced with permission, from Wang et al.[76] Copyright 2020, Wiley.

(B) Schematic illustration of lipid- and ROS-activatable nanoprobe LFP/PCDPD for precise diagnosis and effective therapy of AS. Reproduced with permission, from Wang et al.[74] Copyright 2022, Elsevier.

the signal-to-noise ratio, which can be sequentially activated by ONOO$^-$ and LDs (Figure 10B).[65] Compared with that of control group, the fluorescence intensity of CNP2-B at 517 nm increased with 2600-fold in the presence of LDs mimics and ONOO$^-$, which was attributed to the excellent activation of ONOO$^-$ and LDs. Under the activation of ONOO$^-$, the CNP2-B can be transferred from mitochondria to lipid droplets showing a bright fluorescent signal. Compared with commercial HPF, the CNP2-B can achieve higher specificity and signal-to-noise ratio imaging of atherosclerotic plaques. This research provides important activatable molecular probe tools for the diagnosis and treatment of related diseases.

HClO and ONOO$^-$-Activatable fluorescent probes

The increase of HClO and ONOO$^-$ level is closely related to the initiation and progression of AS.[66] Biomimetic properties of the red blood cell interface can reduce macrophage-mediated phagocytosis in blood and improve nanoprobes accumulation in AS. To accurately diagnose AS plaque sites, Kong et al. developed HClO- and ONOO$^-$-activatable nanoprobes R-Lipo@Cy7/CH1055 by embedding first near-infrared (NIR-I, 650–950 nm) probe Cy7 and second near-infrared (NIR-II, 950–1700 nm) probe CH1055 into red blood cell membrane (RBCM)-based liposomes (Figure 11A).[47,67] In the presence of HClO/ONOO$^-$, the fluorescence signal of Cy7 at 770 nm is quenched, while the fluorescence signal of CH1055 at 940 nm has almost no change. Moreover, NIR-II probes have the characteristics of high tissue penetration depth, low tissue background absorption, high signal-to-noise ratio, and so forth, which are especially suitable for bioimaging.[68] As shown in Figure 11B, *in vivo* experiments demonstrate that ratio nanoprobe R-Lipo@Cy7/CH1055 can achieve the precise AS diagnosis through downward ratiometric fluorescence of Cy7 to CH1055. To further diagnosis and vulnerability risk assessment of atherosclerotic plaques, Kong et al. designed HClO- and ONOO$^-$-activatable nanoprobes FANP@RBCM by embedding amphiphilic amino acid-assembled nanoparticle containing Cy7 and CH1055 into RBCM, showing good biosafety, effective accumulation in atherosclerotic plaques, excellent ratiometric response upon HClO- and ONOO$^-$-activation (Figure 11C).[69] Therefore, the ratiometric probes have broad application prospects for precise identification and vulnerability risk assessment of atherosclerotic plaques.

ACTIVATABLE FLUORESCENT PROBE FOR AS THERAPY

Currently, the main therapeutic strategies for AS are drug therapy and endovascular intervention.[5,12,45] However, traditional drug therapy faces some shortcomings, such as lack of targeting and poor re-endothelialization, resulting in low therapeutic efficacy and high risk of thrombosis.[70] Endovascular intervention can cause some complications, such as thrombosis, myocardial infarction, and so forth.[71] Moreover, AS in the early stage is often asymptomatic and difficult to detect.[72] Therefore, it is urgent to develop new theranostic agents for early diagnosis and effective treatment of AS.
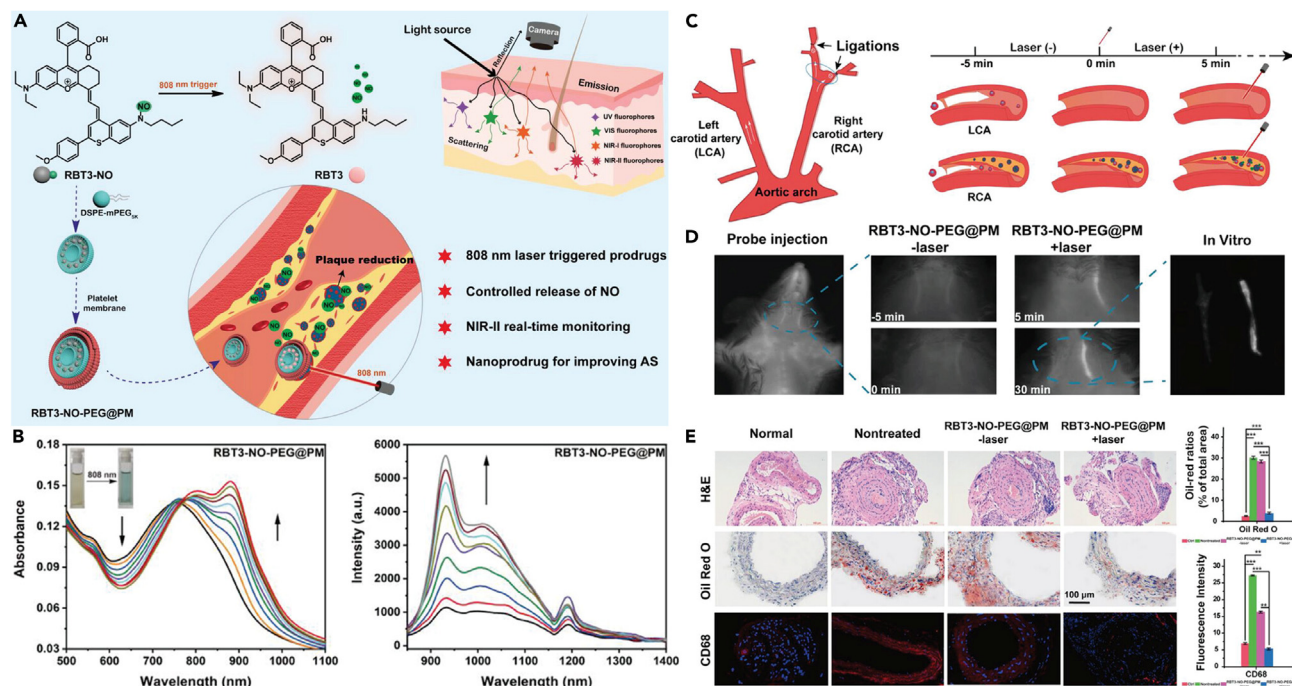
Figure 13. Photoactivatable probe for AS theranostics
(A) Schematic illustration of RBT3-NO-PEG@PM for AS theranostics.
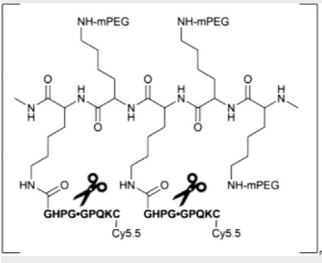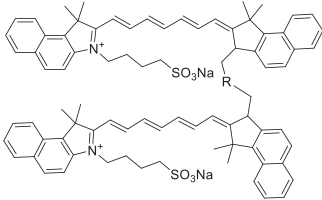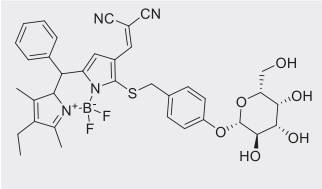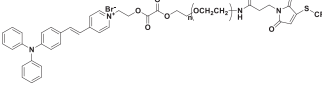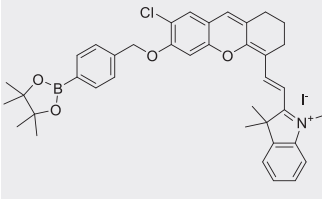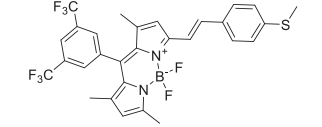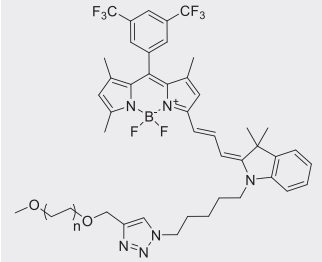(B) The UV–vis absorption and PL spectra of RBT3-NO-PEG@PM under 808 nm laser irradiation for 0–80 min.
(C) Diagrammatic sketch of the model mice.
(D and E) The theranostic potential of RBT3-NO-PEG@PM; Reproduced with permission, from Chai et al.[79] Copyright 2024, Wiley.

Drug delivery systems have broad application prospects in the diagnosis and treatment of early atherosclerosis.[73] Wang et al. developed a theranostic nanoplatform TPCDP@PMM composed of a two-photon AIE probe TP, β-cyclodextrin with ROS responsive bond, anti-inflammatory glucocorticoid and ROS responsive copolymer, which could be used for atherosclerosis theranostics (Figure 12A). However, this drug delivery system is limited by drawbacks such as poor active targeting, toxic side effects caused by systemic distribution, and non-specific recognition. To overcome these challenges, Wang et al. further constructed a lipid- and ROS-activatable therapeutic nanoprobe LFP/PCDPD, exhibiting green fluorescence emission in lipids, red fluorescence emission under physiological environment, specific targeted recognition of atherosclerotic plaques, ROS-responsive drug release and lipid clearance (Figure 12B).[74] LFP/PCDPD could actively target atherosclerotic plaques through the high affinity of Dex to vascular adhesion molecule-1 (VCAM-1) and CD44 receptor, and effectively release the lipid-targeted AIE probe LFP and cyclodextrin with lipid removal function under ROS activation. *In vivo* experiments have confirmed that LFP/PCDPD could precisely identify atherosclerotic plaques and effectively eliminate lipids, enabling precise treatment of AS under imaging guidance. NIR-I probes have some drawbacks such as low tissue penetration depth, poor signal-to-noise ratio, and strong tissue absorption, while NIR-II probes have broader application prospects in the diagnosis and identification of diseases due to high tissue penetration depth, low tissue absorption and high signal-to-noise ratio.[75]
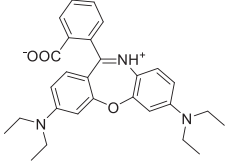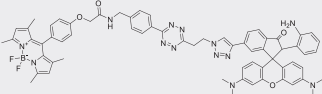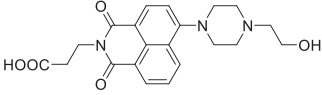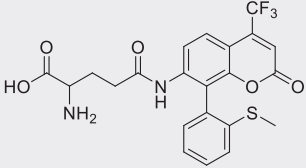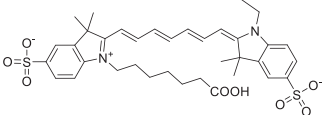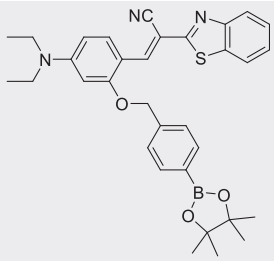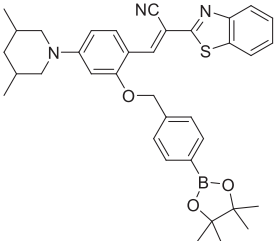
Benefiting from specific localization to macrophage-derived foam cells in atherosclerotic microenvironment, platelets are highly suitable for the precise localization of AS.[77] Due to precise spatiotemporal controllability of light, photoactivatable fluorescent probes can convert from a weakly emission state to a bright fluorescent state through photochemical reactions, and transform from inert prodrugs to active drugs, which can selectively light up the target area and amplify therapeutic effect.[78] In 2024, Chai et al. synthesized a series of photoactivatable fluorescent probes (RBT-NO), which can activate the NIR-II emission and release the NO under 808 nm laser irradiation (Figure 13).[79] Due to the high photoactivatable efficiency, the RBT3-NO is selected for early diagnosis and effective treatment of AS. As shown in Figure 13A, RBT3-NO coated by platelet membrane, namely RBT3-NO-PEG@PM, was used for improving the targeting ability of atherosclerotic plaque sites. Under 808 nm laser irradiation for different time, a decreased absorption signal of RBT3-NO-PEG@PM was observed at 625 nm, while the absorption intensity at 883 nm and PL intensity at 933 nm gradually increased, suggesting the high photoactivatable efficiency (Figure 13B). Next, the model mice of AS were established by ligating right carotid artery (RCA), and the left carotid artery (LCA, normal group) was nontreated (Figure 13C). About 5 min after tail vein injection of RBT3-NO-PEG@PM, weak fluorescent at the RCA was observed, while a significantly increased fluorescence signal at the RCA was exhibited under 808 nm laser irradiation (Figure 13D). Due to the high-precision spatiotemporal control of light, the full release of NO at the atherosclerotic plaques can effectively reduce the lipid deposition (Figure 13E). Therefore, the photoactivatable prodrug RBT3-NO-PEG@PM with targeting ability of atherosclerotic plaques is highly promising for AS theranostics in the future. Although the

Table 1. Summary of activatable fluorescence probes for AS theranostics

Probes	Pathological parameters	λ_{ex} [nm]	Probe types	λ_{em} [nm]	Applications	Year	References
	CTK	670	Turn "on"	720	Visualization of CTK activity in atherosclerosis	2007	Jaffer et al.[33]
	CTB	750	Turn "on"	845	Detection of embolism-vulnerable atherosclerotic plaques	2019	Narita et al.[34]
	β-Gal	633	Turn "on"	727	Imaging of senescent cells/vasculature in AS	2020	Chen et al.[37]
	H$_2$O$_2$	480	Turn "on"	650	Identification of atherosclerotic plaques	2023	Liu et al.[46]
	H$_2$O$_2$	640	Ratio Probe	F_{710}/F_{940}	Ratiometric imaging of H$_2$O$_2$ level in AS	2024	Liu et al.[47]
	HClO	535	Ratio Probe	F_{600}/F_{670}	Identification of atherosclerotic Plaques	2022	Ye et al.[49]
	HClO	460/640	Ratio Probe	F_{540}/F_{740}	Detection of atherosclerosis	2024	Ji et al.[50]

Table 1. Continued

Probes	Pathological parameters	λ_{ex} [nm]	Probe types	λ_{em} [nm]	Applications	Year	References
	ONOO⁻	620	Turn "on"	672	ONOO⁻ sensors in macrophage-derived foam cells	2022	Zhang et al.[54]
	NO	488	Turn "on"	F_{592}/F_{512}	Endogenous NO sensors in atherosclerosis plaques	2023	Zhou et al.[55]
/MOFs (PCN-224)	pH and phosphorylation	380 415	Turn "on"	530 645	Monitor of the pH level and phosphorylation level in the early AS	2023	Li et al.[56]
	GGT and HBrO	380	Ratio Probe	F_{500}/F_{450}	Simultaneous detection of GGT and HBrO in early atherosclerotic plaques	2024	Li et al.[56]
	ONOO⁻ and HClO	710	Ratio Probe	F_{770}/F_{940}	Ratiometric imaging of ONOO⁻ and HClO level in AS	2024	Liu et al.[47]
	ONOO⁻ and LDs	488	Turn "on"	517	Precise intraoperative imaging of atherosclerotic plaques	2023	Sang et al.[64]
	ONOO⁻ and LDs	488	Turn "on"	517	AS imaging	2023	Sang et al.[65]

(Continued on next page)

Table 1. *Continued*

Probes	Pathological parameters	λ_{ex} [nm]	Probe types	λ_{em} [nm]	Applications	Year	References
	Platelet membrane-targeting and photoactivatable	883	Turn "on"	933	AS theranostics	2024	Chai et al.[79]

studies on activatable fluorescent probes with both imaging and therapeutic functions have emerged in the precise diagnosis and treatment of AS, it still requires unremitting efforts to develop activatable NIR-II theranostic probes for imaging-guided precise AS therapy.

CONCLUSION AND OUTLOOK

This review highlights the recent cutting-edge progress of activatable fluorescent probes based on atherosclerotic microenvironment for AS theranostics. Various functional groups responsive to specific biomarkers in the atherosclerotic microenvironment were modified onto the fluorescent backbone to develop mono- and dual-activatable fluorescent probes. Moreover, the photoactivatable fluorescent probes have been used for early diagnosis and effective treatment of AS. Overall, significant development of mono-/dual-activatable fluorescent probes have been exhibited in precise diagnosis and effective therapy of AS (Table 1).

While activatable fluorescent probes based on atherosclerotic microenvironment have made significant progress in the diagnosis and treatment of AS, the excitation and emission of most of the activatable fluorescent probes reported based on atherosclerotic microenvironment are located in the visible (400–700 nm) or first near-infrared (700–900 nm) window, showing low tissue penetration depth, strong biological tissue absorption, scattering and autofluorescence. These drawbacks make it difficult to achieve widespread clinical translation. The microenvironment at various stages of AS development is different, and the expression levels of biomarkers are limited. Thus, the activatable diagnostic and therapeutic probes are partially activated. Although they can diagnose AS, its therapeutic effect is greatly reduced. Therefore, innovative strategies are still needed to construct more intelligent activatable probes. Thus, we put forward several recommendations: (1) Benefiting from high tissue penetration depth, low tissue absorption, and high signal-to-noise ratio, the second near-infrared (NIR-II, 1000–1700 nm) fluorescent probes have broad application prospects in diagnosis.[68] The activatable NIR-II fluorescent probes based on atherosclerotic microenvironment are more conducive to the diagnosis of AS in deep tissue. (2) A single biomarker is not unique to the atherosclerotic microenvironment,[80] so the dual-/multi-activatable fluorescent probes are needed for accurate diagnosis of AS. (3) Reasonable structural modification of activatable fluorescent probes can effectively increase *in vivo* circulation and the targeting ability of AS lesion. (4) The diagnostic identification of AS-specific metabolites is also an effective strategy for rapid diagnosis of AS. (5) The modification of aggregation-induced emission groups can effectively overcome the defect of fluorescence self-quenching in the aggregated state.[81] (6) It is highly promising for the development of multi-activatable NIR-II fluorescent probes based on atherosclerotic microenvironment, which can light up fluorescent signals to locating the lesion sites, and then utilize external stimuli (such as light, sound, magnetism, etc.) to selectively amplify therapeutic effect of AS. In summary, we believe that greater application prospects of activatable fluorescent probes will be achieved in imaging-guided precise AS therapy through reasonable structural modification and extensive research efforts.

AUTHOR CONTRIBUTIONS

Y.Y. and C.T. contributed equally in this work. Conceptualization, Y.Y. and C.T.; writing—original draft preparation, Y.Y. and C.T.; writing—review and editing, Y.Y., C.T., S.L., W.L., Y.L., D.Y., D.W., and X.C.; supervision, X.C.; project administration, Y.Y., X.C., and D.W.; funding acquisition, X.C. and Y.Y. All authors have read and agreed to the published version of the manuscript.

DECLARATION OF INTERESTS

The authors declare no competing interests.

REFERENCES

1. Björkegren, J.L.M., and Lusis, A.J. (2022). Atherosclerosis: recent developments. Cell 185, 1630–1645. https://doi.org/10.1016/j.cell.2022.04.004.

2. Adkar, S.S., and Leeper, N.J. (2024). Efferocytosis in atherosclerosis. Nat. Rev. Cardiol. 135, 1–18. https://doi.org/10.1038/s41569-024-01037-7.

3. Khan, A., Roy, P., and Ley, K. (2024). Breaking tolerance: the autoimmune aspect of atherosclerosis. Nat. Rev. Immunol. 24, 670–679. https://doi.org/10.1038/s41577-024-01010-y.

4. Ma, B., Chen, Z., Xu, H., Sun, S., Huang, C., Li, G., Zhang, W., Shang, M., Wang, Y., and Fu, G. (2024). Biomimetic targeting nanoplatform for atherosclerosis theranostics via photoacoustic diagnosis and "Hand-In-Hand" immunoregulation. Adv. Funct. Mater. 34, 2311305. https://doi.org/10.1002/adfm.202311305.

5. Engelen, S.E., Robinson, A.J.B., Zurke, Y.-X., and Monaco, C. (2022). Therapeutic strategies targeting inflammation and immunity in atherosclerosis: how to proceed? Nat. Rev. Cardiol. 19, 522–542. https://doi.org/10.1038/s41569-021-00668-4.

6. Liu, L., Chen, W., Zhou, H., Duan, W., Li, S., Huo, X., Xu, W., Huang, L., Zheng, H., Liu, J., et al. (2020). Chinese stroke association guidelines for clinical management of cerebrovascular disorders: executive summary and 2019 update of clinical management of ischaemic cerebrovascular diseases. Stroke Vasc. Neurol. 5, 159–176. https://doi.org/10.1136/svn-2020-000378.

7. Song, J.W., Pavlou, A., Xiao, J., Kasner, S.E., Fan, Z., and Messé, S.R. (2021). Vessel wall magnetic resonance imaging biomarkers of symptomatic intracranial atherosclerosis. Stroke 52, 193–202. https://doi.org/10.1161/STROKEAHA.120.031480.

8. Nurmohamed, N.S., van Rosendael, A.R., Danad, I., Ngo-Metzger, Q., Taub, P.R., Ray, K.K., Figtree, G., Bonaca, M.P., Hsia, J., Rodriguez, F., et al. (2024). Atherosclerosis evaluation and cardiovascular risk estimation using coronary computed tomography angiography. Eur. Heart J. 45, 1783–1800. https://doi.org/10.1093/eurheartj/ehae190.

9. Araki, M., Park, S.-J., Dauerman, H.L., Uemura, S., Kim, J.-S., Di Mario, C., Johnson, T.W., Guagliumi, G., Kastrati, A., Joner, M., et al. (2022). Optical coherence tomography in coronary atherosclerosis assessment and intervention. Nat. Rev. Cardiol. 19, 684–703. https://doi.org/10.1038/s41569-022-00687-9.

10. Rioufol, G., Finet, G., Ginon, I., André-Fouët, X., Rossi, R., Vialle, E., Desjoyaux, E., Convert, G., Huret, J.F., and Tabib, A. (2002). Multiple atherosclerotic plaque rupture in acute coronary syndrome: a three-vessel intravascular ultrasound study. Circulation 106, 804–808. https://doi.org/10.1161/01.CIR.0000025609.13806.31.

11. Xie, J., Chen, K., Huang, J., Lee, S., Wang, J., Gao, J., Li, X., and Chen, X. (2010). PET/NIRF/MRI triple functional iron oxide nanoparticles. Biomaterials 31, 3016–3022. https://doi.org/10.1016/j.biomaterials.2010.01.010.

12. Zhang, S., Liu, Y., Cao, Y., Zhang, S., Sun, J., Wang, Y., Song, S., and Zhang, H. (2022). Targeting the microenvironment of vulnerable atherosclerotic plaques: An emerging diagnosis and therapy strategy for atherosclerosis. Adv. Mater. 34, 2110660. https://doi.org/10.1002/adma.202110660.

13. Li, J., Xu, J., Zhang, W., Li, P., Zhang, W., Wang, H., and Tang, B. (2023). Detection and imaging of active substances in early atherosclerotic lesions using fluorescent probes. Chembiochem 24, e202300105. https://doi.org/10.1002/cbic.202300105.

14. Chen, X., Niu, N., Li, D., Zhang, Z., Zhuang, Z., Yan, D., Li, J., Zhao, Z., Wang, D., and Tang, B.Z. (2023). The golden touch by light: A finely engineered luminogen empowering high photoactivatable and photodynamic efficiency for cancer phototheranostics. Adv. Funct. Mater. 33, 2211571. https://doi.org/10.1002/adfm.202211571.

15. Chen, X., Zhang, Z., Luo, W., Zhuang, Z., Zhao, Z., Wang, L., Wang, D., and Tang, B.Z. (2022). A photoactivatable theranostic probe for simultaneous oxidative stress-triggered multi-color cellular imaging and photodynamic therapy. Biomaterials 287, 121680. https://doi.org/10.1016/j.biomaterials.2022.121680.

16. Chen, X., Li, Y., Li, S., Gao, M., Ren, L., and Tang, B.Z. (2018). Mitochondria-and lysosomes-targeted synergistic chemo-photodynamic therapy associated with self-monitoring by dual light-up fluorescence. Adv. Funct. Mater. 28, 1804362. https://doi.org/10.1002/adfm.201804362.

17. Hu, C., Zhang, Z., Sun, S., Liu, H., Yuan, L., and Zhang, X.-B. (2024). Progress and perspective of atherosclerosis-targeted molecular probes: From precise imaging to auxiliary diagnosis and treatment. Coord. Chem. Rev. 510, 215850. https://doi.org/10.1016/j.ccr.2024.215850.

18. Wu, X., Wang, R., Kwon, N., Ma, H., and Yoon, J. (2022). Activatable fluorescent probes for in situ imaging of enzymes. Chem. Soc. Rev. 51, 450–463. https://doi.org/10.1039/d1cs00543j.

19. Wang, X., Ding, Q., Groleau, R.R., Wu, L., Mao, Y., Che, F., Kotova, O., Scanlan, E.M., Lewis, S.E., Li, P., et al. (2024). Fluorescent probes for disease diagnosis. Chem. Rev. 124, 7106–7164. https://doi.org/10.1021/acs.chemrev.3c00776.

20. Mendive-Tapia, L., and Vendrell, M. (2022). Activatable fluorophores for imaging immune cell function. Acc. Chem. Res. 55, 1183–1193. https://doi.org/10.1021/acs.accounts.2c00070.

21. Zhu, J., Zhu, R., and Miao, Q. (2022). Polymeric agents for activatable fluorescence, self-luminescence and photoacoustic imaging. Biosens. Bioelectron. 210, 114330. https://doi.org/10.1016/j.bios.2022.114330.

22. Zheng, J., Zhao, S., Mao, Y., Du, Z., Li, G., and Sang, M. (2022). Lipid-activatable fluorescent probe for intraoperative imaging of atherosclerotic plaque using in situ patch. Small 18, 2104471. https://doi.org/10.1002/smll.202104471.

23. Mei, J., and Tian, H. (2021). Most recent advances on enzyme-activatable optical probes for bioimaging. Aggregate 2, e32. https://doi.org/10.1002/agt2.32.

24. Song, J.W., Ahn, J.W., Lee, M.W., Kim, H.J., Kang, D.O., Kim, R.H., Kang, U.G., Kim, Y.H., Han, J., Park, Y.H., et al. (2021). Targeted theranostic photoactivation on atherosclerosis. J. Nanobiotechnol. 19, 338. https://doi.org/10.1186/s12951-021-01084-z.

25. Qi, Y.L., Li, Y.Z., Tan, M.J., Yuan, F.F., Murthy, N., Duan, Y.T., Zhu, H.L., and Yang, S.Y. (2023). Recent advances in organic near-infrared ratiometric small-molecule fluorescent probes. Coord. Chem. Rev. 486, 215130. https://doi.org/10.1016/j.ccr.2023.215130.

26. Ouyang, J., Sun, L., Zeng, F., and Wu, S. (2022). Biomarker-activatable probes based on smart AIEgens for fluorescence and optoacoustic imaging. Coord. Chem. Rev. 458, 214438. https://doi.org/10.1016/j.ccr.2022.214438.

27. He, J., Zhang, W., Zhou, X., Xu, F., Zou, J., Zhang, Q., Zhao, Y., He, H., Yang, H., and Liu, J. (2023). Reactive oxygen species (ROS)-responsive size-reducible nanoassemblies for deeper atherosclerotic plaque penetration and enhanced macrophage-targeted drug delivery. Bioact. Mater. 19, 115–126. https://doi.org/10.1016/j.bioactmat.2022.03.041.

28. Hou, J.-T., Yu, K.-K., Sunwoo, K., Kim, W.Y., Koo, S., Wang, J., Ren, W.X., Wang, S., Yu, X.-Q., and Kim, J.S. (2020). Fluorescent imaging of reactive oxygen and nitrogen species associated with pathophysiological processes. Chem 6, 832–866. https://doi.org/10.1016/j.chempr.2019.12.005.

29. Chen, W., Schilperoort, M., Cao, Y., Shi, J., Tabas, I., and Tao, W. (2022). Macrophage-targeted nanomedicine for the diagnosis and treatment of atherosclerosis. Nat. Rev. Cardiol. 19, 228–249. https://doi.org/10.1038/s41569-021-00629-x.

30. Bilbrough, T., Piemontese, E., and Seitz, O. (2022). Dissecting the role of protein phosphorylation: a chemical biology toolbox. Chem. Soc. Rev. 51, 5691–5730. https://doi.org/10.1039/d1cs00991e.

31. Choudhury, R.P., Fuster, V., and Fayad, Z.A. (2004). Molecular, cellular and functional imaging of atherothrombosis. Nat. Rev. Drug Discov. 3, 913–925. https://doi.org/10.1038/nrd1548.

32. Weiss-Sadan, T., Gotsman, I., and Blum, G. (2017). Cysteine proteases in atherosclerosis. FEBS J. 284, 1455–1472. https://doi.org/10.1111/febs.14043.

33. Jaffer, F.A., Kim, D.-E., Quinti, L., Tung, C.-H., Aikawa, E., Pande, A.N., Kohler, R.H., Shi, G.-P., Libby, P., and Weissleder, R. (2007). Optical visualization of cathepsin K activity in atherosclerosis with a novel, protease-activatable fluorescence sensor. Circulation 115, 2292–2298. https://doi.org/10.1161/CIRCULATIONAHA.106.660340.

34. Narita, Y., Shimizu, K., Ikemoto, K., Uchino, R., Kosugi, M., Maess, M.B., Magata, Y., Oku, N., and Ogawa, M. (2019). Macrophage-targeted, enzyme-triggered fluorescence switch-on system for detection of embolism-vulnerable atherosclerotic plaques. J. Control. Release 302, 105–115. https://doi.org/10.1016/j.jconrel.2019.03.025.

35. Childs, B.G., Durik, M., Baker, D.J., and van Deursen, J.M. (2015). Cellular senescence in aging and age-related disease: From mechanisms to therapy. Nat. Med. 21, 1424–1435. https://doi.org/10.1038/nm.4000.

36. Debacq-Chainiaux, F., Erusalimsky, J.D., Campisi, J., and Toussaint, O. (2009). Protocols to detect senescence-associated beta-galactosidase (SA-βgal) activity, a biomarker of senescent cells in culture and in vivo. Nat. Protoc. 4, 1798–1806. https://doi.org/10.1038/nprot.2009.191.

37. Chen, J.A., Guo, W., Wang, Z., Sun, N., Pan, H., Tan, J., Ouyang, Z., Fu, W., Wang, Y., Hu, W., and Gu, X. (2020). In vivo imaging of senescent vascular cells in atherosclerotic

mice using a β-galactosidase-activatable nanoprobe. Anal. Chem. *92*, 12613–12621. https://doi.org/10.1021/acs.analchem.0c02670.

38. Hou, J.-T., Zhang, M., Liu, Y., Ma, X., Duan, R., Cao, X., Yuan, F., Liao, Y.-X., Wang, S., and Xiu Ren, W. (2020). Fluorescent detectors for hydroxyl radical and their applications in bioimaging: A review. Coord. Chem. Rev. *421*, 213457. https://doi.org/10.1016/j.ccr.2020.213457.

39. Zhang, Z., Fan, J., Du, J., and Peng, X. (2021). Two-channel responsive luminescent chemosensors for dioxygen species: Molecular oxygen, singlet oxygen and superoxide anion. Coord. Chem. Rev. *427*, 213575. https://doi.org/10.1016/j.ccr.2020.213575.

40. Pang, E., Zhao, S., Wang, B., Niu, G., Song, X., and Lan, M. (2022). Strategies to construct efficient singlet oxygen-generating photosensitizers. Coord. Chem. Rev. *472*, 214780. https://doi.org/10.1016/j.ccr.2022.214780.

41. Gao, W., Li, X., Liu, Z., Fu, W., Sun, Y., Cao, W., Tong, L., and Tang, B. (2019). A redox-responsive self-assembled nanoprobe for photoacoustic inflammation imaging to assess atherosclerotic plaque vulnerability. Anal. Chem. *91*, 1150–1156. https://doi.org/10.1021/acs.analchem.8b04912.

42. Gui, L., Yan, J., Zhao, J., Wang, S., Ji, Y., Liu, J., Wu, J., Yuan, K., Liu, H., Deng, D., and Yuan, Z. (2023). Hypochlorite activatable ratiometric fluorescent probe based on endoplasmic reticulum stress for imaging of atherosclerosis. Biosens. Bioelectron. *240*, 115660. https://doi.org/10.1016/j.bios.2023.115660.

43. Xu, H., She, P., Zhao, Z., Ma, B., Li, G., and Wang, Y. (2023). Duplex responsive nanoplatform with cascade targeting for atherosclerosis photoacoustic diagnosis and multichannel combination therapy. Adv. Mater. *35*, 2300439. https://doi.org/10.1002/adma.202300439.

44. Zhou, Y., Hou, D., Marigo, C.C., Bonelli, J., Rocas, P., Cheng, F., Yang, X., Rocas, J., Hamberg, N.M., and Han, J. (2022). Redox-responsive polyurethane-polyurea nanoparticles targeting to aortic endothelium and atherosclerosis. iScience *25*, 105390. https://doi.org/10.1016/j.isci.2022.105390.

45. Liu, Y., Jiang, Z., Yang, X., Wang, Y., Yang, B., and Fu, Q. (2024). Engineering nanoplatforms for theranostics of atherosclerotic plaques. Adv. Healthcare Mater. *13*, 2303612. https://doi.org/10.1002/adhm.202303612.

46. Liu, J., He, Z., Zhong, Y., Zhu, L., Yan, M., Mou, N., Qu, K., Qin, X., Wang, G., Zhang, K., et al. (2023). Reactive oxygen species-responsive sequentially targeted AIE fluorescent probe for precisely identifying the atherosclerotic plaques. ACS Appl. Mater. Interfaces *15*, 47381–47393. https://doi.org/10.1021/acsami.3c09573.

47. Liu, B., Han, G.M., Wang, D.X., Liu, D.B., Liu, A.A., Wang, J., Xiao, Y.L., Yuan, L., and Kong, D.M. (2024). Red blood cell membrane biomimetic nanoprobes for ratiometric imaging of reactive oxygen species level in atherosclerosis. Chem. Eng. J. *479*, 147515. https://doi.org/10.1016/j.cej.2023.147515.

48. Cui, K., Zhang, D., Zhang, G., and Zhu, D. (2010). A highly selective naked-eye probe for hypochlorite with the p-methoxyphenol-substituted aniline compound. Tetrahedron

Lett. *51*, 6052–6055. https://doi.org/10.1016/j.tetlet.2010.09.041.

49. Ye, Z., Ji, M., Wu, K., Yang, J., Liu, A.A., Sun, W., Ding, D., and Liu, D. (2022). In-sequence high-specificity dual-reporter unlocking of fluorescent probe enables the precise identification of atherosclerotic plaques. Angew. Chem. Int. Ed. Engl. *61*, e202204518. https://doi.org/10.1002/anie.202204518.

50. Ji, M., Wei, Y., Ye, Z., Hong, X., Yu, X., Du, R., Li, Q., Sun, W., and Liu, D. (2024). In vivo fluorescent labeling of foam cell-derived extracellular vesicles as circulating biomarkers for in vitro detection of atherosclerosis. J. Am. Chem. Soc. *146*, 10093–10102. https://doi.org/10.1021/jacs.4c01173.

51. Pi, S., Mao, L., Chen, J., Shi, H., Liu, Y., Guo, X., Li, Y., Zhou, L., He, H., Yu, C., et al. (2021). The P2RY12 receptor promotes VSMC-derived foam cell formation by inhibiting autophagy in advanced atherosclerosis. Autophagy *17*, 980–1000. https://doi.org/10.1080/15548627.2020.1741202.

52. Grootaert, M.O.J., and Bennett, M.R. (2021). Vascular smooth muscle cells in atherosclerosis: time for a re-assessment. Cardiovasc. Res. *117*, 2326–2339. https://doi.org/10.1093/cvr/cvab046.

53. Laval, T., and Ouimet, M. (2023). A role for lipophagy in atherosclerosis. Nat. Rev. Cardiol. *20*, 431–432. https://doi.org/10.1038/s41569-023-00885-z.

54. Zhang, H., Xu, Y., Li, H., Shi, W., Li, X., and Ma, H. (2022). New rhodamines with changeable π-conjugation for lengthening fluorescence wavelengths and imaging peroxynitrite. Chem *8*, 287–295. https://doi.org/10.1016/j.chempr.2021.11.023.

55. Zhou, L., Wang, Z., Wang, L., Zhang, X., and Xiao, Y. (2023). Tetrazine-based ratiometric nitric oxide sensor identifies endogenous nitric oxide in atherosclerosis plaques by riding macrophages as a smart vehicle. J. Am. Chem. Soc. *145*, 28296–28306. https://doi.org/10.1021/jacs.3c12181.

56. Li, J., Zhao, N., Zhang, W., Li, P., Yin, X., Zhang, W., Wang, H., and Tang, B. (2023). Assessing the progression of early atherosclerosis mice using a fluorescence nanosensor for the simultaneous detection and imaging of pH and phosphorylation. Angew. Chem., Int. Ed. Engl. *62*, e202215178. https://doi.org/10.1002/anie.202215178.

57. Forman, H.J., and Zhang, H. (2021). Targeting oxidative stress in disease: Promise and limitations of antioxidant therapy. Nat. Rev. Drug Discov. *20*, 689–709. https://doi.org/10.1038/s41573-021-00233-1.

58. Yan, H., Huo, F., Yue, Y., Chao, J., and Yin, C. (2021). Rapid reaction, slow dissociation aggregation, and synergetic multicolor emission for imaging the restriction and regulation of biosynthesis of Cys and GSH. J. Am. Chem. Soc. *143*, 318–325. https://doi.org/10.1021/jacs.0c10840.

59. Yan, K.C., Sedgwick, A.C., Zang, Y., Chen, G.R., He, X.P., Li, J., Yoon, J., and James, T.D. (2019). Sensors, imaging agents, and theranostics to help understand and treat reactive oxygen species related diseases. Small Methods *3*, 1900013. https://doi.org/10.1002/smtd.201900013.

60. Wang, H., Zhang, X., Li, P., Huang, F., Xiu, T., Wang, H., Zhang, W., Zhang, W., and Tang, B. (2024). Prediction of early atherosclerotic plaques using a sequence-activated fluorescence probe for the simultaneous detection of γ-glutamyl transpeptidase and

hypobromous acid. Angew. Chem., Int. Ed. Engl. *63*, e202315861. https://doi.org/10.1002/anie.202315861.

61. Sang, M., Cai, B., Qin, S., Zhao, S., Mao, Y., Wang, Y., Yu, X., and Zheng, J. (2021). Lipid droplet-specific probe for rapidly locating atherosclerotic plaques and intraoperative imaging via in situ spraying. ACS Appl. Mater. Interfaces *13*, 58369–58381. https://doi.org/10.1021/acsami.1c17797.

62. Wang, Z., Wang, S., Wang, B., Shen, J., Zhao, L., Yu, F., and Hou, J.-T. (2023). A two-pronged detection of atherosclerosis with a dual-channel fluorescent probe for viscosity and hypochlorous acid. Chem. Eng. J. *464*, 142687. https://doi.org/10.1016/j.cej.2023.142687.

63. Gao, M., Tang, M., Ho, W., Teng, Y., Chen, Q., Bu, L., Xu, X., and Zhang, X.-Q. (2023). Modulating plaque inflammation via targeted mRNA nanoparticles for the treatment of atherosclerosis. ACS Nano *17*, 17721–17739. https://doi.org/10.1021/acsnano.3c00958.

64. Sang, M., Huang, Y., Liu, Z., Li, G., Wang, Y., Yuan, Z., Dai, C., and Zheng, J. (2023). Peroxynitrite/lipid droplet sequence-activated dual-lock fluorescent probes enable precise intraoperative imaging of atherosclerotic plaques. ACS Sens. *8*, 893–903. https://doi.org/10.1021/acssensors.2c02590.

65. Sang, M., Huang, Y., Wang, L., Chen, L., Zheng, J., Nawsherwan, Li, G., Li, G., Wang, Y., Yu, X., and Dai, C. (2023). An "AND" molecular logic gate as a super-enhancers for de novo designing activatable probe and its application in atherosclerosis imaging. Adv. Sci. *10*, 2207066. https://doi.org/10.1002/advs.202207066.

66. Hansson, G.K. (2017). Inflammation and atherosclerosis. Circulation *136*, 1875–1877. https://doi.org/10.1161/circulationaha.117.030484.

67. Chen, L., Lyu, Y., Zhang, X., Zheng, L., Li, Q., Ding, D., Chen, F., Liu, Y., Li, W., Zhang, Y., et al. (2023). Molecular imaging: design mechanism and bioapplications. Sci. China Chem. *66*, 1336–1383. https://doi.org/10.1007/s11426-022-1461-3.

68. Qin, Y., Chen, X., Gui, Y., Wang, H., Tang, B.Z., and Wang, D. (2022). Self-assembled metallacage with second near-infrared aggregation-induced emission for enhanced multimodal theranostics. J. Am. Chem. Soc. *144*, 12825–12833. https://doi.org/10.1021/jacs.2c03895.

69. Han, G.M., Liu, B., Wang, C.Y., Wang, D.X., Li, Q.N., Cai, Q.L., and Kong, D.M. (2024). Diagnosis and vulnerability risk assessment of atherosclerotic plaques using an amino acid-assembled near-infrared ratiometric nanoprobe. Anal. Chem. *96*, 10380–10390. https://doi.org/10.1021/acs.analchem.4c01487.

70. Libby, P. (2021). The changing landscape of atherosclerosis. Nature *592*, 524–533. https://doi.org/10.1038/s41586-021-03392-8.

71. Soehnlein, O., and Libby, P. (2021). Targeting inflammation in atherosclerosis—from experimental insights to the clinic. Nat. Rev. Drug Discov. *20*, 589–610. https://doi.org/10.1038/s41573-021-00198-1.

72. Tarkin, J.M., Dweck, M.R., Evans, N.R., Takx, R.A.P., Brown, A.J., Tawakol, A., Fayad, Z.A., and Rudd, J.H.F. (2016). Imaging atherosclerosis. Circ. Res. *118*, 750–769. https://doi.org/10.1161/CIRCRESAHA.115.306247.

73. Luby, B.M., Charron, D.M., MacLaughlin, C.M., and Zheng, G. (2017). Activatable fluorescence: From small molecule to nanoparticle. Adv. Drug Deliv. Rev. *113*, 97–121. https://doi.org/10.1016/j.addr.2016.08.010.

74. Xu, H., She, P., Ma, B., Zhao, Z., Li, G., and Wang, Y. (2022). ROS responsive nanoparticles loaded with lipid-specific AIEgen for atherosclerosis-targeted diagnosis and bifunctional therapy. Biomaterials *288*, 121734. https://doi.org/10.1016/j.biomaterials.2022.121734.

75. Pan, W., Rafiq, M., Haider, W., Guo, Y., Wang, H., Xu, M., Yu, B., Cong, H., and Shen, Y. (2024). Recent advances in NIR-II fluorescence/photoacoustic dual-modality imaging probes. Coord. Chem. Rev. *514*, 215907. https://doi.org/10.1016/j.ccr.2024.215907.

76. Ma, B., Xu, H., Zhuang, W., Wang, Y., Li, G., and Wang, Y. (2020). ROS responsive nanoplatform with two-photon AIE imaging for atherosclerosis diagnosis and "two-pronged" therapy. Small *16*, 2003253. https://doi.org/10.1002/smll.202003253.

77. Ma, C., Li, Y., Tian, M., Deng, Q., Qin, X., Lu, H., Gao, J., Chen, M., Weinstein, L.S., Zhang, M., et al. (2024). Gsα regulates macrophage foam cell formation during atherosclerosis. Circ. Res. *134*, e34–e51. https://doi.org/10.1161/CIRCRESAHA.123.323156.

78. You, Y., Tang, C., Lin, S., Zeng, D., Cong, Y., Wang, D., and Chen, X. (2023). Photoactivatable aggregation-induced emission luminogens based on photodehydrogenation reactions for biomedical applications. Luminescence *39*, e4645. https://doi.org/10.1002/bio.4645.

79. Chai, Y., Shangguan, L., Yu, H., Sun, Y., Huang, X., Zhu, Y., Wang, H.-Y., and Liu, Y. (2024). Near infrared light-activatable platelet-mimicking NIR-II NO nano-prodrug for precise atherosclerosis theranostics. Adv. Sci. *11*, 2304994. https://doi.org/10.1002/advs.202304994.

80. Duan, Q.J., Zhao, Z.Y., Zhang, Y.J., Fu, L., Yuan, Y.Y., Du, J.Z., and Wang, J. (2023). Activatable fluorescent probes for real-time imaging-guided tumor therapy. Adv. Drug Deliv. Rev. *196*, 114793. https://doi.org/10.1016/j.addr.2023.114793.

81. Kang, M., Zhang, Z., Song, N., Li, M., Sun, P., Chen, X., Wang, D., and Tang, B.Z. (2020). Aggregation-enhanced theranostics: AIE sparkles in biomedical field. Aggregate *1*, 80–106. https://doi.org/10.1002/agt2.7.